International Journal of Mechanical Sciences 214 (2022) 106873

Contents lists available at ScienceDirect

International Journal of Mechanical Sciences

journal homepage: www.elsevier.com/locate/ijmecsci

Dynamic analysis and non-standard continualization of a Timoshenko beam lattice

F. Gómez-Silva *, R. Zaera

Department of Continuum Mechanics and Structural Analysis, University Carlos III of Madrid, Avda. de la Universidad, 30., Leganés, Madrid 28911, Spain

ARTICLE INFO

Keywords:
Timoshenko beam lattice
Dispersive behaviour
Continualization
Pseudo-differential operator
Transition frequency
Natural frequencies

ABSTRACT

In this paper, a Timoshenko beam lattice, made up of a chain of masses and straight segments, is proposed, considering bending and shear deformation by means of linear rotational and transverse springs, respectively. Different standard and non-standard continualization methods are applied to it, highlighting here for the first time the suitability of taking the coupled discrete governing equations as a starting point for deriving new continuum models. Several novel low order non-classical continuum models are obtained, with the aim of reliably capturing size-effects and reflecting the dispersive behaviour of the discrete system. Low order governing equations prevents the need for extra boundary conditions when finite (bounded) solids are treated. An extensive analysis of the transition frequency, which initiates the shear propagation spectrum, has been carried out, examining its influence for the discrete and non-standard continuum models. The natural frequencies of a finite solid with two different boundary conditions are obtained through an edge treatment applied here for the first time to this kind of lattices, thus making it possible to solve the *clamped-free* edges configuration. The reliability of these approaches is evaluated by comparing their dynamic behaviours with that of the discrete system (taken as a reference), through both dispersion and vibration analyses, some of the new proposed continuum models successfully capturing the behaviour of the discrete one, even for high wavenumbers. Moreover, the appearance of physical inconsistencies is examined.

1. Introduction

Size-effects appear in problems where the microstructure is roughly in size to the characteristic length of the phenomenon under study. These are present in a variety of microscale engineering problems such as robotics [1–4] and biosensors fields [5–7], where nano- and micro-electromechanical systems are used [8–10], as well as in macro-scale problems like in wave propagation through composites [11–14] or metamaterials [15–18].

Molecular Dynamics and Lattice Dynamics approaches are theories commonly adopted to understand the dynamic behaviour of solids at different relevant scales. They arise as an alternative to classical continuum models, which although widely used in engineering problems, are scale-length free and their formulation fails when size-effects (due to matter being essentially discrete) are present. Even if they capture size-effects with high accuracy, these approaches require a high computational cost to be solved. This is why, since the 19th century (works by Cauchy and Voigt), considerable efforts have been devoted to obtaining non-classical continuum models, capable of capturing size-effects as accurately as possible, with a lower computational cost. Despite the fact that Mindlin [19], Eringen [20,21] or Toupin [22], among others, carried out the first attempts in the 1960s, the interest in these theories remains to this day with non-local models [23–25], and developing works in which modified couple stress and strain gradient formulation are applied in order to study the behaviour of rods [26–28], beams [29–32], shells [33–35] or plates [36–38]. Nevertheless, all these models are considered axiomatic, which depend on non-classical constants, whose value requires to be calibrated by experimental results. As an alternative to the axiomatic models, the continualization of discrete systems appears. These systems are made up of periodically repeating cells, whose mechanical and geometrical properties are related to the scale parameters of the new continuum models. Bacigalupo and Gambarotta [39] carry out a comprehensive comparative study on the application of standard and non-standard continualization procedures in some one- and two-dimensional lattice systems.

The Born-Von Kármán lattice, consisting of a one-dimensional chain of identical masses connected through linear springs, is one of the simplest models to understand the size-effects in the discrete matter. This model has been continualized using a comprehensive range of

* Corresponding author.
E-mail address: frgomezs@ing.uc3m.es (F. Gómez-Silva).

https://doi.org/10.1016/j.ijmecsci.2021.106873
Received 25 May 2021; Received in revised form 15 September 2021; Accepted 11 October 2021
Available online 28 October 2021

Nomenclature

$\overline{x}_n$	Dimensionless discrete position
$\overline{x}$	Dimensionless continuous position
τ	Dimensionless time variable
$\overline{v}_n$	Dimensionless discrete displacement
$\overline{v}$	Dimensionless continuous displacement
θ_n	Discrete rotation of the segment
θ	Continuous rotation
d	Characteristic length of the lattice
N	Number of segments in the lattice
C	Stiffness of the rotational springs
S	Stiffness of the transverse springs
m	Mass of particles
I_b	Rotational inertia of the segments
α	Dimensionless ratio between stiffness parameters
β	Dimensionless ratio between inertial parameters
Ω	Dimensionless wave frequency
$\overline{K}$	Dimensionless wavenumber
$\overline{v}_g$	Dimensionless group velocity
$\overline{\mathscr{L}}$	Dimensionless Lagrangian
$\overline{T}$	Dimensionless kinetic energy
$\overline{T}_d$	Dimensionless kinetic energy density
$\overline{W}$	Dimensionless potential energy
$\overline{W}_d$	Dimensionless potential energy density
$\partial_{\overline{x}}$	Dimensionless spatial derivative
a_i	Scale parameters of continuum models (i=1,...,5)
λ	Beam slenderness
E	Young modulus
G	Shear modulus
I	Second moment of area
A	Cross section area
κ	Timoshenko shear coefficient
ρ	Density
$V(\overline{x})$	Vibration mode for transverse continuous displacement
A_i	Integration constants for $V(\overline{x})$ ($i = 1,\ldots,4$)
V_n	Vibration mode for transverse displacement of the particle n
B_i	Integration constants for V_n ($i = 1,\ldots,4$)
Ω_{trans}	Transition frequency

procedures, both standard and non-standard methods, leading to the classical rod equation if the higher-order derivatives are disregarded. Polyzos and Fotiadis [40] applied different standard methods to it, including distributed mass in the springs of the chain. Gómez-Silva et al. [41] add next-nearest interactions to the Born-Von Kármán lattice and employ different standard and non-standard continualization techniques.

Within the context of beam lattices, Challamel et al. [42–44] and Wang et al. [45,46] propose a system composed of masses equally spaced by straight segments connected by linear rotational springs, expanding it to obtain non-local equivalent continua for buckling and vibration analysis of microstructured beams. Bacigalupo and Gambarotta [47] solve some thermodynamic inconsistencies that appear when deriving equivalent models of periodic beam-lattice materials through standard continualization methods. Gómez-Silva and Zaera [48] develop different non-classical models, employing both standard and non-standard continualization methods, searching for low-order governing equation, and analysing the influence of boundary conditions. Moreover, they propose in [49] a system including next-nearest interactions, deriving new non-classical continuum models, and performing an in-depth analysis of the edge treatment. On the other hand, non-classical Timoshenko models can be developed by considering shear deformations through transverse linear springs, as suggested by Duan et al. in [50]. In that work, they apply a non-standard continualization to it, using Padé approximant, and they obtain the natural frequencies for the discrete model with simply-supported ends. Zhang et al. [51] perform a buckling analysis in a Timoshenko beam lattice for the simply-supported problem.

Within the framework of nonlinear discrete systems, Barchiesi et al. [52] study systems that include both bending and shear deformation, considering large displacements. Discretization of beam models is often used to describe the internal structure of mechanical metamaterials [53], which are currently generating a great interest [54,55]. Nevertheless, some of these schemes present relevant drawbacks, particularly when considering large deformation regimes. Turco et al. [56] propose a discretization scheme based on the Timoshenko continuum formulation [57], in order to solve these issues. In a subsequent work, Turco et al. [58] apply some of these ideas to the dynamic study of a pantographic beam, which enable the design of materials with tailored properties. Nonlinear size-dependent models are also employed for the study of microelectromechanical systems (MEMS) with large defection, such as electrostatically actuated microcantilever beams, in which a phenomenon known as pull-in instability appears [59,60]. Nonetheless, linear size-dependent models are also widely studied and applied in fields such as mass-detection, in nanomechanical systems like nanobeams resonators [61,62].

In this work, the Timoshenko beam system proposed in [50], considering small displacements, is revisited. Different continualization procedures (standard and non-standard) are proposed and applied for the first time to this kind of system. The possibility of taking the uncoupled discrete governing equation as a starting point for deriving non-classical continuum models is discussed, concluding that it may lead to some inconsistencies. Furthermore, the capability of the proposed non-classical continuum models in capturing the behaviour of the discrete model, considered as a reference, is evaluated. For this purpose, the dispersion relations of all models are analysed (in the case of unbounded solids), differentiating between the propagation of bending and shear waves. A detailed study of the transition frequency, above which shear deformation modes appear, has been carried out, analysing its influence on the discrete and non-standard continuum models. In addition, the natural frequencies (in the case of bounded solids) for the simply-supported and clamped-free configurations are obtained. In this case, only the models derived from non-standard continualization methods are compared with the discrete one, since they provide low-order governing equations, thus avoiding the need for extra boundary conditions to be considered. Inconsistencies in the new continuum models are examined, and an analysis of the edge treatment is carried out, proposing a novel approach for the boundary conditions, based on central difference schemes.

This paper is structured as follows. In Section 2, the discrete model is defined and its dispersion relation is obtained. In Section 3, all the proposed continualization procedures, both standard and non-standard, are explained, obtaining the dispersion relations of the new non-classical models and discussing the application of these procedures to the uncoupled discrete governing equation. In addition, the equivalence between discrete and continuum parameters is found. The influence of edge conditions is studied in Section 4. In Section 5, a thorough analysis of the transition frequency is performed. Subsequently, the results are discussed in Section 6, comparing the dispersion curves and natural frequencies of the obtained continuum models with those of the discrete ones. Finally, some concluding remarks are listed in Section 7.

2. Discrete reference model

In this section, the Timoshenko lattice system proposed by Duan et al. [50] is presented. The dynamic behaviour of this system, that will be called discrete model, is considered as a reference in this work. The system consists of a discrete chain of length L, built up by N straight segments, whose translational inertia is lumped into single particles of mass m, as it can be seen in Fig. 1. These segments have a length $d = L/N$, which is considered as the characteristic length scale of the lattice, and are connected by linear elastic rotational and transverse springs of stiffness C and S, respectively. The vertical position of a particle n, $n = 0, \ldots, N$, is determined by its vertical displacement $v_n(t)$, t being the time variable, whereas its horizontal coordinate (fixed) is defined as $x_n = nd$. In Fig. 1(a) and (b), the reference and deformed configurations are shown, respectively. If small displacements of the particles are considered, it can be assumed that $\cos\theta = 1$, $\sin\theta = \theta$ and $d + \Delta d = d$. Keeping this in mind, the total elastic potential energy of the chain is

$$W = \frac{1}{2}\sum_{n=1}^{N} S(\Delta l_n)^2 + \frac{1}{2}\sum_{n=1}^{N} C(\Delta\theta_n)^2, \tag{1}$$

where $\Delta l_n = v_n - v_{n-1} - d\,\theta_{n-1}$ and $\Delta\theta_n = \theta_n - \theta_{n-1}$ are the variations of length and angle of transversal and rotational springs, respectively.

The total kinetic energy of the chain is

$$T = \frac{1}{2}\sum_{n=0}^{N} m\left(\frac{\partial v_n}{\partial t}\right)^2 + \frac{1}{2}\sum_{n=1}^{N} I_b\left(\frac{\partial\theta_n}{\partial t}\right)^2, \tag{2}$$

where I_b is the rotational inertia of the straight segments. Thus, the Lagrangian of the system can be defined as $\mathscr{L} = T - W$. By means of the Euler-Lagrange equations

$$\frac{\partial\mathscr{L}}{\partial v_n} = \frac{d}{dt}\left(\frac{\partial\mathscr{L}}{\partial\dot{v}_n}\right); \tag{3}$$

$$\frac{\partial\mathscr{L}}{\partial\theta_n} = \frac{d}{dt}\left(\frac{\partial\mathscr{L}}{\partial\dot{\theta}_n}\right), \tag{4}$$

where $\dot{v}_n$ and $\dot{\theta}_n$ are the transversal and rotational discrete velocities, the following discrete governing equations are obtained

$$S\left(v_{n+1} - 2v_n + v_{n-1}\right) - Sd\left(\theta_n - \theta_{n-1}\right) = m\frac{\partial^2 v_n}{\partial t^2}; \tag{5}$$

$$C\left(\theta_{n+1} - 2\theta_n + \theta_{n-1}\right) + Sd\left(v_{n+1} - v_n - d\theta_n\right) = I_b\frac{\partial^2\theta_n}{\partial t^2}, \tag{6}$$

which can be rewritten in dimensionless form as

$$\left(\overline{v}_{n+1} - 2\overline{v}_n + \overline{v}_{n-1}\right) - \left(\theta_n - \theta_{n-1}\right) = \alpha\frac{\partial^2\overline{v}_n}{\partial\tau^2}; \tag{7}$$

$$\alpha\left(\theta_{n+1} - 2\theta_n + \theta_{n-1}\right) + \left(\overline{v}_{n+1} - \overline{v}_n - \theta_n\right) = \alpha\beta\frac{\partial^2\theta_n}{\partial\tau^2}, \tag{8}$$

where

$$\overline{v}_n = \frac{v_n}{d}; \quad \tau = \widetilde{\omega}t; \quad \widetilde{\omega} = \sqrt{\frac{C}{md^2}}; \quad \alpha = \frac{C}{Sd^2}; \quad \beta = \frac{I_b}{md^2}. \tag{9}$$

Considering $F_n = \theta_n - \theta_{n-1}$ and $M_n = \overline{v}_{n+1} - 2\overline{v}_n + \overline{v}_{n-1}$, Eq. (7) can be expressed compactly as

$$M_n - F_n = \alpha\frac{\partial^2\overline{v}_n}{\partial\tau^2}. \tag{10}$$

If the index of Eq. (8) is shifted by one, it leads to

$$\alpha\left(\theta_n - 2\theta_{n-1} + \theta_{n-2}\right) + \left(\overline{v}_n - \overline{v}_{n-1} - \theta_{n-1}\right) = \alpha\beta\frac{\partial^2\theta_{n-1}}{\partial\tau^2}. \tag{11}$$

Now, by subtracting Eq. (11) from Eq. (8), the next uncoupled equation is obtained

$$\alpha\left(F_{n+1} - 2F_n + F_{n-1}\right) + \left(M_n - F_n\right) = \alpha\beta\frac{\partial^2 F_n}{\partial\tau^2}. \tag{12}$$

With the intention of eliminating F_{n+1}, F_n and F_{n-1}, Eq. (10) is introduced in Eq. (12), achieving the following compact discrete governing equation

$$\begin{aligned}(M_{n+1} - 2M_n + M_{n-1}) - \alpha\left(\frac{\partial^2\overline{v}_{n+1}}{\partial\tau^2} - 2\frac{\partial^2\overline{v}_n}{\partial\tau^2} + \frac{\partial^2\overline{v}_{n-1}}{\partial\tau^2}\right)\\ + \frac{\partial^2\overline{v}_n}{\partial\tau^2} - \beta\left(\frac{\partial^2 M_n}{\partial\tau^2} - \alpha\frac{\partial^4\overline{v}_n}{\partial\tau^4}\right) = 0,\end{aligned} \tag{13}$$

which can be written in displacements terms as

$$\begin{aligned}\left(\overline{v}_{n+2} - 4\overline{v}_{n+1} + 6\overline{v}_n - 4\overline{v}_{n-1} + \overline{v}_{n-2}\right) - (\alpha+\beta)\left(\frac{\partial^2\overline{v}_{n+1}}{\partial\tau^2} - 2\frac{\partial^2\overline{v}_n}{\partial\tau^2} + \frac{\partial^2\overline{v}_{n-1}}{\partial\tau^2}\right)\\ + \frac{\partial^2\overline{v}_n}{\partial\tau^2} + \beta\alpha\frac{\partial^4\overline{v}_n}{\partial\tau^4} = 0.\end{aligned} \tag{14}$$

The dispersion relation of this model can be obtained by assuming the plane wave solution

$$\overline{v}_n(\tau) = v_0 e^{i\left(\Omega\tau - \overline{K}\overline{x}_n\right)}, \tag{15}$$

where $\overline{K} = Kd$ and $\Omega = \omega/\widetilde{\omega}$ are the dimensionless wavenumber and wave frequency, being ω and K their dimensional counterparts, respectively, and $\overline{x}_n = x_n/d = n$, $n = 0, \ldots, N$, is the dimensionless horizontal position of a particle n. Introducing Eq. (15) in Eq. (14) the following dispersion equation (two branches) is found

$$\Omega = \sqrt{\frac{1 - (\alpha+\beta)R_1 \pm \sqrt{(1-(\alpha+\beta)R_1)^2 - 4\alpha\beta R_2}}{2\alpha\beta}}, \tag{16}$$

where

$$R_1 = 2\cos\left(\overline{K}\right) - 2; \quad R_2 = 2\cos\left(2\overline{K}\right) - 8\cos\left(\overline{K}\right) + 6. \tag{17}$$

As it can be seen, this dispersion relation depends on the dimensionless parameters α and β. In order to test the trend of the dynamic behaviour of the system, its dispersion curves are presented in Fig. 2 for different values of α, adopting a value $\alpha/3$ for the parameter β (the rationale for this choice of the value of β is based on the similarities between the classical Timoshenko beam theory and the continuum models derived from the discrete one, as it will be explained below). Note that the dispersion relation of the discrete model is periodic of period 2π and symmetric with respect to the axis $\overline{K} = \pi$, so it is of interest exclusively in the Irreducible Brillouin Zone (IBZ), $0 < \overline{K} < \pi$. The first set of dispersion curves, plotted in Fig. 2(a), corresponds to the propagation of bending waves and tends to the Euler-Bernoulli spectrum when $\alpha \to 0$. The second set, plotted in Fig. 2(b), corresponds to the propagation of shear waves and tends to $\Omega = (\alpha\beta)^{-1/2}$ when $\overline{K} \to 0$. Moreover, as it can be proven through Eq. (16), it tends to infinity when $\alpha \to 0$ (infinite stiffness of shear springs) for the whole range of $\overline{K}$.

3. Continualization methods

Despite the fact that the discrete model captures the size-effects, and

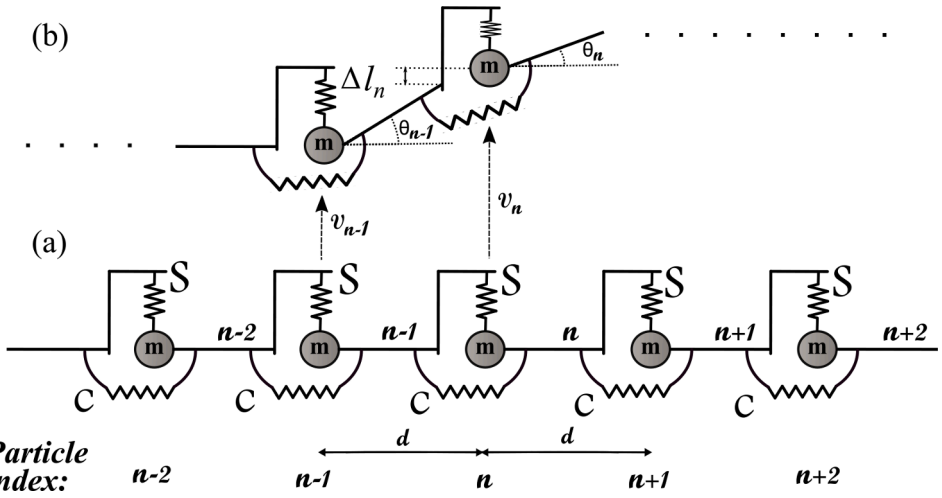

Fig. 1. Timoshenko beam lattice system made up of a chain of length L formed by $N+1$ particles with mass m and N straight segments of length $d = L/N$, joined by linear elastic rotational (bending deformation) and transverse (shear deformation) springs of stiffness C and S, respectively. (a) Reference configuration. (b) Deformed configuration. Vertical position determined by the vertical displacement, $v_n(t)$.

accurately reflects the dynamic behaviour of the lattice, it requires a high computational cost to be solved. For this reason, different continualization methods are applied to the discrete model, in order to achieve continuum models, reproducing the intrinsic dispersive behaviour of the lattice as closely as possible. In this work, it is sought that the governing equations of such continuum models are of low order, since they do not need extra boundary conditions with complex physical interpretation to be considered when finite solids are treated.

3.1. Standard methods

These continualization procedures consist in expanding the discrete variables by means of Taylor's series as follows

$$Y_{n\pm q} = Y(\bar{x},\tau) \pm \frac{\partial Y(\bar{x},\tau)}{\partial \bar{x}} q + \frac{1}{2}\frac{\partial^2 Y(\bar{x},\tau)}{\partial \bar{x}^2} q^2 \pm \frac{1}{6}\frac{\partial^3 Y(\bar{x},\tau)}{\partial \bar{x}^3} q^3 + \frac{1}{24}\frac{\partial^4 Y(\bar{x},\tau)}{\partial \bar{x}^4} q^4 \pm O\left(\frac{\partial^5}{\partial \bar{x}^5}\right); \qquad q = 1,2, \tag{18}$$

where Y_n, Y can be either $\bar{v}_n$, $\bar{v}$ or θ_n, θ, and $\bar{x} = x/d$, $\bar{v} = v/d$ and θ are the continuous horizontal coordinate, displacement and rotation variables, respectively, such that $\bar{v}_n(\tau) = \bar{v}(\bar{x}_n,\tau)$, $\theta_n(\tau) = \theta(\bar{x}_n,\tau)$. Note that when considering dimensionless variables, the characteristic length adopts the unit value, its presence not being immediately noticeable [48,63]. For this reason, the approximation order of Eq. (18) is determined by the order of the dimensionless spatial derivative.

Eq. (18) will be used in three different ways. Firstly, it will be applied to the Lagrangian of the system before using the Hamilton's Principle. Secondly, it is used in the coupled discrete governing equations, giving rise to two continuum governing equations, formally identical to those obtained previously, involving only different values of the scale factors. Finally, the discrete displacement variables are expanded in the uncoupled governing Eq. (14), giving rise to one continuum governing equation in the displacement variables. These models will be named in the rest of this work as *Standard I, II* and *III* models, respectively.

3.1.1. Standard I

In this section, the discrete energy of one unit cell of the system is expanded, as Polyzos and Fotiadis [40] proposed for axial discrete systems. In this case, we make use of the unit cell shown in Fig. 3, which includes the particle with index $n+1$ and the segment n. Then, its dimensionless potential energy per unit length reads

$$\overline{W}_d = \frac{1}{2}\left(\bar{v}_{n+1} - \bar{v}_n - \theta_n\right)^2 + \frac{\alpha}{2}(\theta_{n+1} - \theta_n)^2, \tag{19}$$

where $\overline{W}_d = W_d/(Sd)$, W_d being its dimensional counterpart. Eq. (19) can be expanded via Taylor's series up to second order, leading to

$$\overline{W}_d = \frac{1}{2}\left(\frac{\partial \bar{v}}{\partial \bar{x}} + \frac{1}{2}\frac{\partial^2 \bar{v}}{\partial \bar{x}^2} - \theta\right)^2 + \frac{\alpha}{2}\left(\frac{\partial \theta}{\partial \bar{x}} + \frac{1}{2}\frac{\partial^2 \theta}{\partial \bar{x}^2}\right)^2. \tag{20}$$

Considering the continualized dimensionless classic kinetic energy per unit length

$$\overline{T}_d = \frac{1}{2}\alpha\left(\frac{\partial \bar{v}}{\partial \tau}\right)^2 + \frac{1}{2}\alpha\beta\left(\frac{\partial \theta}{\partial \tau}\right)^2, \tag{21}$$

where $\overline{T}_d = T_d/(Sd)$, and T_d is its dimensional counterpart, the dimensionless Lagrangian of this whole system becomes

$$\overline{\mathscr{L}} = \int_0^N \left(\overline{T}_d - \overline{W}_d\right) d\bar{x}. \tag{22}$$

where $\overline{\mathscr{L}} = \mathscr{L}/(Sd^2)$, $\mathscr{L}$ being its dimensional counterpart. Applying the Hamilton's Principle, the following governing equations are obtained

$$\left(\frac{\partial^2 \bar{v}}{\partial \bar{x}^2} - a_1\frac{\partial^4 \bar{v}}{\partial \bar{x}^4}\right) - \left(\frac{\partial \theta}{\partial \bar{x}} - a_2\frac{\partial^2 \theta}{\partial \bar{x}^2}\right) = \alpha\frac{\partial^2 \bar{v}}{\partial \tau^2}; \tag{23}$$

$$\alpha\left(\frac{\partial^2 \theta}{\partial \bar{x}^2} - a_1\frac{\partial^4 \theta}{\partial \bar{x}^4}\right) + \left(\frac{\partial \bar{v}}{\partial \bar{x}} + a_2\frac{\partial^2 \bar{v}}{\partial \bar{x}^2} - \theta\right) = \alpha\beta\frac{\partial^2 \theta}{\partial \tau^2}, \tag{24}$$

where two scale factor a_1 and a_2 are introduced

$$a_1 = \frac{1}{4}; \quad a_2 = \frac{1}{2}. \tag{25}$$

In order to obtain the dispersion relation of this model, the next plane wave solutions are assumed

$$\bar{v}(t) = Ae^{i\left(\Omega\tau - \bar{K}\bar{x}\right)}; \tag{26}$$

$$\theta(t) = Be^{i\left(\Omega\tau - \bar{K}\bar{x}\right)}, \tag{27}$$

leading to

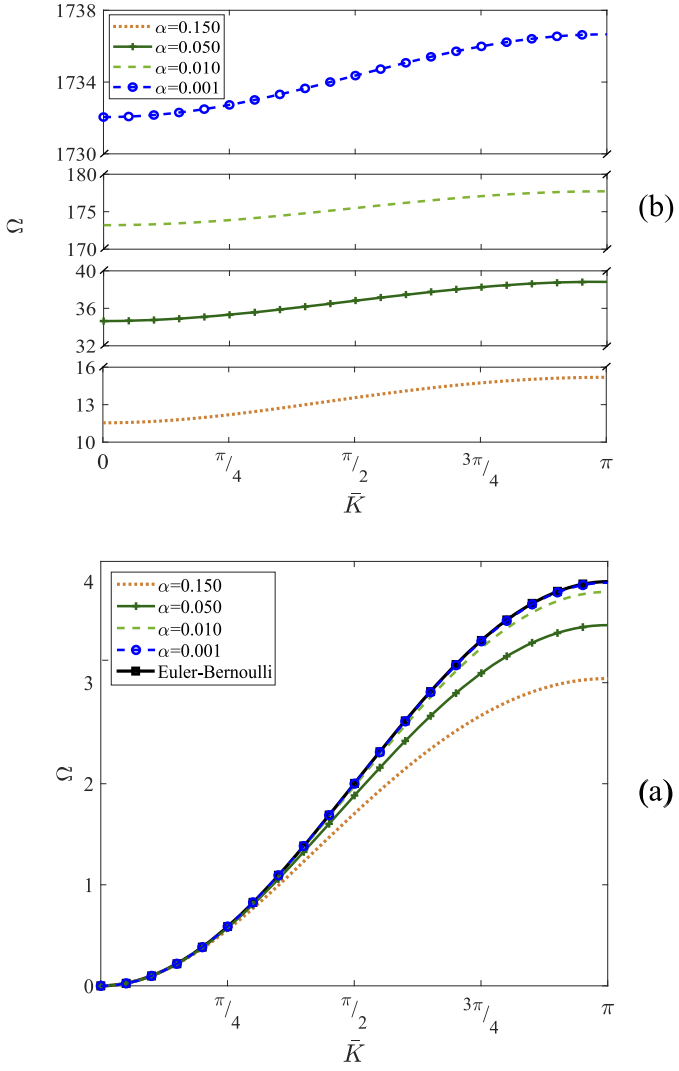

Fig. 2. Dispersion curves of the discrete model for different values of α. Representation of dimensionless frequency Ω vs. wavenumber $\overline{K}$ within the IBZ. (a) Propagation of bending waves and comparison with the dispersion curve of the Euler-Bernoulli lattice beam system [48] ($\alpha = 0$; infinite shear stiffness). (b) Propagation of shear waves, with Ω tending to infinity as $\alpha \to 0$.

$$\begin{pmatrix} -\overline{K}^2 - a_1\overline{K}^4 + \alpha\Omega^2 & -\overline{K}i - a_2\overline{K}^2 \\ \overline{K}i - a_2\overline{K}^2 & -\alpha\overline{K}^2 - \alpha a_1\overline{K}^4 - 1 + \alpha\beta\Omega^2 \end{pmatrix} \begin{pmatrix} A \\ B \end{pmatrix} = \begin{pmatrix} 0 \\ 0 \end{pmatrix}. \tag{28}$$

Obtaining the non-trivial solution of Eq. (28), the following dispersion equation is achieved

$$\Omega = \sqrt{\frac{-b_2 \pm \sqrt{b_2^2 - 4b_1b_3}}{2b_1}}, \tag{29}$$

where

$$b_1 = \alpha\beta; \tag{30}$$

$$b_2 = -\left(\alpha + \beta\right)\left(\overline{K}^2 + a_1\overline{K}^4\right) - 1; \tag{31}$$

$$b_3 = \left(1 + \frac{a_1 - a_2^2}{\alpha}\right)\overline{K}^4 + 2a_1\overline{K}^6 + a_1^2\overline{K}^8. \tag{32}$$

Note that $a_1 - a_2^2 = 0$ for this model. On the other hand, it can be proven how, disregarding the scale parameters ($a_1 = a_2 = 0$), the following governing equations are obtained

$$\frac{\partial^2\overline{v}}{\partial\overline{x}^2} - \frac{\partial\theta}{\partial\overline{x}} = \alpha\frac{\partial^2\overline{v}}{\partial\tau^2}; \tag{33}$$

$$\alpha\frac{\partial^2\theta}{\partial\overline{x}^2} + \frac{\partial\overline{v}}{\partial\overline{x}} - \theta = \alpha\beta\frac{\partial^2\theta}{\partial\tau^2}, \tag{34}$$

which coincide with those of the classical Timoshenko beam theory.

3.1.2. Standard II

Now, the discrete variables are expanded in the *coupled* governing equations of the discrete model. Employing Taylor's series up to fourth order in Eqs. (7) and (8), it results in

$$\left(\frac{\partial^2\overline{v}}{\partial\overline{x}^2} - a_1\frac{\partial^4\overline{v}}{\partial\overline{x}^4}\right) - \left(\frac{\partial\theta}{\partial\overline{x}} - a_2\frac{\partial^2\theta}{\partial\overline{x}^2} + a_3\frac{\partial^3\theta}{\partial\overline{x}^3} - a_4\frac{\partial^4\theta}{\partial\overline{x}^4}\right) = \alpha\frac{\partial^2\overline{v}}{\partial\tau^2}; \tag{35}$$

$$\alpha\left(\frac{\partial^2\theta}{\partial\overline{x}^2} - a_1\frac{\partial^4\theta}{\partial\overline{x}^4}\right) + \left(\frac{\partial\overline{v}}{\partial\overline{x}} + a_2\frac{\partial^2\overline{v}}{\partial\overline{x}^2} + a_3\frac{\partial^3\overline{v}}{\partial\overline{x}^3} + a_4\frac{\partial^4\overline{v}}{\partial\overline{x}^4} - \theta\right) = \alpha\beta\frac{\partial^2\theta}{\partial\tau^2}, \tag{36}$$

where

$$a_1 = -\frac{1}{12}; \quad a_2 = \frac{1}{2}; \quad a_3 = \frac{1}{6}; \quad a_4 = \frac{1}{24}, \tag{37}$$

thus appearing two new scale factors a_2 and a_3. Assuming the plane wave solutions, Eqs. (26) and (27), and obtaining the non-trivial solution, the dispersion relation is given by Eq. (29), the expressions of b_1, b_2 and b_3 being in this case

$$b_1 = \alpha\beta; \tag{38}$$

$$b_2 = -\left(\alpha + \beta\right)\left(\overline{K}^2 + a_1\overline{K}^4\right) - 1; \tag{39}$$

$$b_3 = \left(1 + \frac{a_1 - a_2^2 + 2a_3}{\alpha}\right)\overline{K}^4 + \left(2a_1 + \frac{2a_4a_2 - a_3^2}{\alpha}\right)\overline{K}^6 + a_1^2\overline{K}^8. \tag{40}$$

Note that $a_1 - a_2^2 + 2a_3 = 0$ for this model, and its dispersion relation is formally equivalent to that of the Standard I model, the difference being in the values of the scale parameters and in the expressions of b_i.

3.1.3. Standard III

In this section, the discrete displacement variables are expanded until eighth order directly in the *uncoupled* Eq. (14), while the acceleration variables are expanded up to the sixth order, to obtain a dispersion relation comparable to that of the previous models. Taking this into account, it results in

$$\frac{\partial^4\overline{v}}{\partial\overline{x}^4} + c_1\frac{\partial^6\overline{v}}{\partial\overline{x}^6} + c_2\frac{\partial^8\overline{v}}{\partial\overline{x}^8} - (\alpha+\beta)\left(\frac{\partial^4\overline{v}}{\partial\overline{x}^2\partial\tau^2} + a_1\frac{\partial^6\overline{v}}{\partial\overline{x}^4\partial\tau^2}\right) + \frac{\partial^2\overline{v}}{\partial\tau^2} + \beta\alpha\frac{\partial^4\overline{v}}{\partial\tau^4} = 0, \tag{41}$$

where

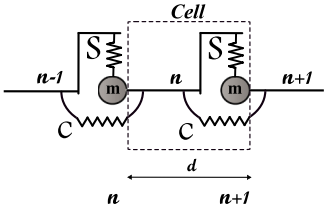

Fig. 3. Unit cell of the lattice system with length d, employed to obtain the non-classical potential energy density, Eq. (19), used in the Standard I model. The cell includes the rotational spring which relates the segments with indices n and $n+1$, and the transverse spring connecting the particle with index $n+1$ and the segment with index n.

$$a_1 = \frac{1}{12}; \quad c_1 = \frac{1}{6}; \quad c_2 = \frac{1}{80}. \tag{42}$$

Assuming the plane wave solution given by Eq. (26), the dispersion relation given by Eq. (29) can be obtained, the expressions of b_1, b_2 and b_3 being in this case

$$b_1 = \alpha\beta; \tag{43}$$

$$b_2 = -\left(\alpha+\beta\right)\left(\overline{K}^2 + a_1\overline{K}^4\right) - 1; \tag{44}$$

$$b_3 = \overline{K}^4 + c_1\overline{K}^6 + c_2\overline{K}^8. \tag{45}$$

This dispersion relation is formally identical to that of the two previous models, and the difference is again in the value of the scale parameters and in the expressions of b_i. Interestingly, the coefficient c_1 of $\overline{K}^6$ in the expression of b_3 is equal to $2a_1$, as it occurs in the Standard I model, and in the Standard II model if $a_3 = a_4 = 0$. However, it does not occur with the coefficient c_2 of $\overline{K}^8$, whose value does not correspond to a_1^2. Thus, the governing equation derived by continualization of the uncoupled discrete Eq. (14) does not comply with the governing equation that would be obtained by uncoupling the continualized coupled equations (e.g. Eqs. (35) and (36)). Therefore, although the uncoupled discrete governing equation is helpful for studying the dynamic behaviour of the lattice system, it should not be used as a starting point to derive the continuum models. It has been verified that this problem occurs using both standard and non-standard continualization methods, making the expansion of Eq. (14) inconsistent.

3.2. Non-standard methods

In this section, the discrete displacement and rotation variables will be expanded by means of the shift operator [41]

$$Y_{n\pm p} = \overline{E}^{\pm p} Y_n; \qquad p = 1, 2, \tag{46}$$

where

$$\overline{E} = \sum_{h=0}^{\infty} \frac{1}{h!}\left(\partial_{\overline{x}}\right)^h = e^{\partial_{\overline{x}}}, \tag{47}$$

$\partial_{\overline{x}}$ referring to the dimensionless spatial derivative. This pseudo-differential operator is going to be employed in three different ways in this work. Firstly, it is applied to the coupled governing equations of the discrete model and expanded subsequently using the Regularization method proposed by Bacigalupo and Gambarotta [64] for discrete systems different than the one considered here. Afterwards, two Enriched Kinetic Energy (EKE) models are proposed, which are obtained by approximating the first spatial derivative by means of difference schemes, and then applying the shift operator to them. The first one employs a progressive differences scheme as proposed by Rosenau [65] for axial systems. The second uses a central differences scheme, as proposed by Gómez-Silva and Zaera [49,73] for a beam lattice with next-nearest interactions. For the remainder of this paper, these models will be referred to as *Regularization, EKE I* and *EKE II* models.

3.2.1. Regularization model

Firstly, Eq. (46) is introduced in Eqs. (7) and (8), leading to

$$\left(e^{\partial_{\overline{x}}} - 2 + e^{-\partial_{\overline{x}}}\right)\overline{v}_n - \left(1 - e^{-\partial_{\overline{x}}}\right)\theta_n = \alpha\frac{\partial^2\overline{v}_n}{\partial\tau^2}; \tag{48}$$

$$\alpha\left(e^{\partial_{\overline{x}}} - 2 + e^{-\partial_{\overline{x}}}\right)\theta_n + \left(e^{\partial_{\overline{x}}} - 1\right)\overline{v}_n - \theta_n = \alpha\beta\frac{\partial^2\theta_n}{\partial\tau^2}. \tag{49}$$

Now, the discrete variables are continualized using the Regularization method proposed by Bacigalupo and Gambarotta [64], which makes use of a central difference scheme and of the shift operator to expand the first spatial derivative as

$$\partial_{\overline{x}} Y|_{x_n} = \frac{Y_{n+1} - Y_{n-1}}{2} = \frac{e^{\partial_{\overline{x}}} - e^{-\partial_{\overline{x}}}}{2} Y_n, \tag{50}$$

thus obtaining the next equation, which relates both discrete and continuous fields

$$Y_n = \frac{2\partial_{\overline{x}}}{e^{\partial_{\overline{x}}} - e^{-\partial_{\overline{x}}}} Y|_{x_n}. \tag{51}$$

Introducing Eq. (51) into the pseudo-differential Eqs. (48) and (49), it leads to

$$P_1\overline{v} - P_2\theta = \alpha\frac{\partial^2 P_3\overline{v}}{\partial\tau^2}; \tag{52}$$

$$\alpha P_1\theta + P_4\overline{v} - P_3\theta = \alpha\beta\frac{\partial^2 P_3\theta}{\partial\tau^2}, \tag{53}$$

where

$$P_1 = \frac{2\partial_{\overline{x}}\left(e^{\partial_{\overline{x}}} - 2 + e^{-\partial_{\overline{x}}}\right)}{e^{\partial_{\overline{x}}} - e^{-\partial_{\overline{x}}}}; \tag{54}$$

$$P_2 = \frac{2\partial_{\overline{x}}\left(1 - e^{-\partial_{\overline{x}}}\right)}{e^{\partial_{\overline{x}}} - e^{-\partial_{\overline{x}}}}; \tag{55}$$

$$P_3 = \frac{2\partial_{\overline{x}}}{e^{\partial_{\overline{x}}} - e^{-\partial_{\overline{x}}}}; \tag{56}$$

$$P_4 = \frac{2\partial_{\overline{x}}\left(e^{\partial_{\overline{x}}} - 1\right)}{e^{\partial_{\overline{x}}} - e^{-\partial_{\overline{x}}}}. \tag{57}$$

In order to obtain low-order continuum governing equations, the above expressions are expanded via Taylor's series until second or fourth order as follows

$$P_1 = \partial_{\overline{x}}^2 + O\left(\partial_{\overline{x}}^4\right); \tag{58}$$

$$P_2 = \partial_{\overline{x}} + O\left(\partial_{\overline{x}}^2\right); \tag{59}$$

$$P_3 = 1 - \frac{1}{6}\partial_{\overline{x}}^2 + O\left(\partial_{\overline{x}}^4\right); \tag{60}$$

$$P_4 = \partial_{\overline{x}} + O\left(\partial_{\overline{x}}^2\right). \tag{61}$$

Eqs. (48) and (49) resulting in

$$\frac{\partial^2\overline{v}}{\partial\overline{x}^2} - \frac{\partial\theta}{\partial\overline{x}} = \alpha\left(\frac{\partial^2\overline{v}}{\partial\tau^2} - a_5\frac{\partial^4\overline{v}}{\partial\overline{x}^2\partial\tau^2}\right); \tag{62}$$

$$\alpha\frac{\partial^2\theta}{\partial\overline{x}^2} + \frac{\partial\overline{v}}{\partial\overline{x}} - \theta = \alpha\beta\left(\frac{\partial^2\theta}{\partial\tau^2} - a_5\frac{\partial^4\theta}{\partial\overline{x}^2\partial\tau^2}\right), \tag{63}$$

where

$$a_5 = \frac{1}{6}. \tag{64}$$

In this model, a new scale parameter a_5 appears, which increases its compliance. Moreover, the scale parameters a_1 to a_4 are not present in this model, hence avoiding higher-order derivatives. Assuming the plane wave solutions given by Eqs. (26) and (27) and keeping the non-trivial solution, the dispersion relation given by Eq. (29) is obtained, the expressions of b_1, b_2 and b_3 being in this case

$$b_1 = \alpha\beta\left(1 + 2a_5\overline{K}^2 + a_5^2\overline{K}^4\right); \tag{65}$$

$$b_2 = -\left(\alpha+\beta\right)\left(\overline{K}^2 + a_5\overline{K}^4\right) - 1 - a_5\overline{K}^2; \tag{66}$$

$$b_3 = \overline{K}^4. \tag{67}$$

3.2.2. Enriched Kinetic Energy I (EKE I) model

In this section, a model derived from the enriched kinetic energy proposed by Rosenau [65,66] for axial vibrating systems is employed. This continualization procedure is applied here to the proposed lattice, which consists in expanding the displacement and rotation variables of the kinetic energy of the discrete model. The first spatial derivative of the continuous variables can be calculated with a progressive difference scheme, and using the shift operator, as

$$\partial_{\overline{x}} Y|_{x_n} = Y_{n+1} - Y_n = \left(e^{\partial_{\overline{x}}} - 1\right) Y_n, \tag{68}$$

thus obtaining the following expression that relates both discrete and continuous fields

$$Y_n = \frac{2\partial_{\overline{x}}}{e^{\partial_{\overline{x}}} - 1} Y|_{x_n}, \tag{69}$$

which can be rewritten through trigonometric identities as

$$Y_n = \frac{\partial_{\overline{x}}}{\cosh\left(\partial_{\overline{x}}\right) + \sinh\left(\partial_{\overline{x}}\right) - 1} Y|_{\overline{x}}. \tag{70}$$

If Eq. (70) is expanded by Taylor's series until second order (in order to achieve a low order governing equation), the next relation between both continuous and discrete variables is obtained

$$Y_n = Q_1 Y, \tag{71}$$

where

$$Q_1 = 1 - \frac{1}{2}\partial_{\overline{x}} + \frac{1}{12}\partial_{\overline{x}}^2 + O\left(\partial_{\overline{x}}^4\right). \tag{72}$$

By means of Eq. (71), the kinetic energy density of the system can be written as (see Appendix A for more details)

$$\overline{T}_d = \frac{1}{2}\alpha\left[\left(\frac{\partial\overline{v}}{\partial\tau}\right)^2 + \frac{1}{12}\left(\frac{\partial^2\overline{v}}{\partial\overline{x}\partial\tau}\right)^2\right] + \frac{1}{2}\alpha\beta\left[\left(\frac{\partial\theta}{\partial\tau}\right)^2 + \frac{1}{12}\left(\frac{\partial^2\theta}{\partial\overline{x}\partial\tau}\right)^2\right]. \tag{73}$$

On the other hand, the discrete potential energy Eq. (19) can be expanded by low order Taylor's series (classic potential energy) as

$$\overline{W}_d = \frac{1}{2}\left(\frac{\partial\overline{v}}{\partial\overline{x}} - \theta\right)^2 + \frac{1}{2}\alpha\left(\frac{\partial\theta}{\partial\overline{x}}\right)^2. \tag{74}$$

Applying the Hamilton's Principle to the Lagrangian of this model, defined by Eq. (22), the following governing equations are obtained

$$\frac{\partial^2\overline{v}}{\partial\overline{x}^2} - \frac{\partial\theta}{\partial\overline{x}} = \alpha\left(\frac{\partial^2\overline{v}}{\partial\tau^2} - a_5\frac{\partial^4\overline{v}}{\partial\overline{x}^2\partial\tau^2}\right); \tag{75}$$

$$\alpha\frac{\partial^2\theta}{\partial\overline{x}^2} + \frac{\partial\overline{v}}{\partial\overline{x}} - \theta = \alpha\beta\left(\frac{\partial^2\theta}{\partial\tau^2} - a_5\frac{\partial^4\theta}{\partial\overline{x}^2\partial\tau^2}\right), \tag{76}$$

where

$$a_5 = \frac{1}{12}. \tag{77}$$

These equations are formally equivalent to Eqs. (62) and (63), the difference being the value of a_5. Therefore, the dispersion relation of this model is provided by Eq. (29), the expressions of b_1, b_2 and b_3 being given by Eqs. (65) to (67).

3.2.3. Enriched Kinetic Energy (EKE) model II

Now, the continualization method proposed by Gómez-Silva and Zaera [49] for an Euler-Bernoulli lattice with next-nearest interactions is applied to the lattice proposed in this work. In this case, the central difference scheme given by Eq. (50) is used to expand the discrete variables of the kinetic energy density, instead of the progressive difference scheme employed in the EKE I model. Hence, using trigonometric functions in Eq. (51), the following expression, relating both continuous and discrete variables, can be obtained

$$Y_n = \frac{\partial_{\overline{x}}}{\sinh\left(\partial_{\overline{x}}\right)} Y|_{\overline{x}}. \tag{78}$$

Eq. (78) can be expanded by Taylor series up to second order, following the same approach as in the previous model, leading to

$$Y_n = Q_2 Y, \tag{79}$$

where

$$Q_2 = 1 - \frac{1}{6}\partial_{\overline{x}}^2 + O\left(\partial_{\overline{x}}^4\right). \tag{80}$$

By means of Eq. (79), the following kinetic energy density can be obtained (see Appendix A for more details)

$$\overline{T}_d = \frac{1}{2}\alpha\left[\left(\frac{\partial\overline{v}}{\partial\tau}\right)^2 + \frac{1}{3}\left(\frac{\partial^2\overline{v}}{\partial\overline{x}\partial\tau}\right)^2\right] + \frac{1}{2}\alpha\beta\left[\left(\frac{\partial\theta}{\partial\tau}\right)^2 + \frac{1}{3}\left(\frac{\partial^2\theta}{\partial\overline{x}\partial\tau}\right)^2\right]. \tag{81}$$

If the classic potential energy given by Eq. (74) is considered, the following governing equations can be obtained applying the Hamilton's Principle

$$\frac{\partial^2\overline{v}}{\partial\overline{x}^2} - \frac{\partial\theta}{\partial\overline{x}} = \alpha\left(\frac{\partial^2\overline{v}}{\partial\tau^2} - a_5\frac{\partial^4\overline{v}}{\partial\overline{x}^2\partial\tau^2}\right); \tag{82}$$

$$\alpha\frac{\partial^2\theta}{\partial\overline{x}^2} + \frac{\partial\overline{v}}{\partial\overline{x}} - \theta = \alpha\beta\left(\frac{\partial^2\theta}{\partial\tau^2} - a_5\frac{\partial^4\theta}{\partial\overline{x}^2\partial\tau^2}\right), \tag{83}$$

where

$$a_5 = \frac{1}{3}. \tag{84}$$

These equations are also formally equivalent to Eqs. (62) and (63), the difference again being the value of a_5, so the dispersion relation of this model is given by Eq. (29), where the expressions of b_1, b_2 and b_3 are provided by Eqs. (65) to (67).

In order to collect the results obtained by the different continualization techniques presented above, the following general governing and dispersion equations are used

$$\left(\frac{\partial^2\overline{v}}{\partial\overline{x}^2} - a_1\frac{\partial^4\overline{v}}{\partial\overline{x}^4}\right) - \left(\frac{\partial\theta}{\partial\overline{x}} - a_2\frac{\partial^2\theta}{\partial\overline{x}^2} + a_3\frac{\partial^3\theta}{\partial\overline{x}^3} - a_4\frac{\partial^4\theta}{\partial\overline{x}^4}\right) = \alpha\left(\frac{\partial^2\overline{v}}{\partial\tau^2} - a_5\frac{\partial^4\overline{v}}{\partial\overline{x}^2\partial\tau^2}\right); \tag{85}$$

$$\alpha\left(\frac{\partial^2\theta}{\partial\overline{x}^2} - a_1\frac{\partial^4\theta}{\partial\overline{x}^4}\right) + \left(\frac{\partial\overline{v}}{\partial\overline{x}} + a_2\frac{\partial^2\overline{v}}{\partial\overline{x}^2} + a_3\frac{\partial^3\overline{v}}{\partial\overline{x}^3} + a_4\frac{\partial^4\overline{v}}{\partial\overline{x}^4} - \theta\right) = \alpha\beta\left(\frac{\partial^2\theta}{\partial\tau^2} - a_5\frac{\partial^4\theta}{\partial\overline{x}^2\partial\tau^2}\right); \tag{86}$$

$$\Omega = \sqrt{\frac{-b_2 \pm \sqrt{b_2^2 - 4b_1b_3}}{2b_1}}, \tag{87}$$

where

$$b_1 = \alpha\beta\left(1 + 2a_5\overline{K}^2 + a_5^2\overline{K}^4\right); \tag{88}$$

$$b_2 = -\left(\alpha + \beta\right)\left(\overline{K}^2 + \left(a_1 + a_5\right)\overline{K}^4\right) - 1 - a_5\overline{K}^2; \tag{89}$$

$$b_3 = \left(1 + \frac{a_1 - a_2^2 + 2a_3}{\alpha}\right)\overline{K}^4 + \left(2a_1 + \frac{2a_4a_2 - a_3^2}{\alpha}\right)\overline{K}^6 + a_1^2\overline{K}^8, \tag{90}$$

which depend on the scale parameters a_1 to a_5, whose values are presented for each model in Table 1.

3.3. Equivalence between discrete and continuum parameters

In this section, we are going to look for the equivalence between the inertial and stiffness parameters that describe a solid continuum beam and those of the discrete model. For this purpose, the governing equations of the continualized Classical model (Eqs. (33) and (34)), written in dimensional form

$$Sd\left(\frac{\partial^2 v}{\partial x^2}-\frac{\partial \theta}{\partial x}\right)=\frac{m}{d}\frac{\partial^2 v}{\partial t^2}; \tag{91}$$

$$Cd\frac{\partial^2 \theta}{\partial x^2}+Sd\left(\frac{\partial v}{\partial x}-\theta\right)=\frac{I_b}{d}\frac{\partial^2 \theta}{\partial t^2}, \tag{92}$$

are formally compared with the classical Timoshenko beam equations

$$\kappa AG\left(\frac{\partial^2 v}{\partial x^2}-\frac{\partial \theta}{\partial x}\right)=\rho A\frac{\partial^2 v}{\partial t^2}; \tag{93}$$

$$EI\frac{\partial^2 \theta}{\partial x^2}+\kappa AG\left(\frac{\partial v}{\partial x}-\theta\right)=\rho I\frac{\partial^2 \theta}{\partial t^2}, \tag{94}$$

finding out the following equivalences

$$S=\frac{\kappa AG}{d}; \quad C=\frac{EI}{d}; \quad m=\rho Ad; \quad I_b=\rho Id, \tag{95}$$

where E, I, A, G, κ and ρ are the elastic modulus, the second moment of area, the cross-section area, the shear modulus, the Timoshenko shear coefficient and the density of the beam, respectively. Bearing it in mind, the following equivalence between dimensional and dimensionless frequencies arise

$$\omega=\sqrt{\frac{C}{md^2}}\Omega=N^2\sqrt{\frac{EI}{\rho AL^4}}\Omega, \tag{96}$$

where the number of segments N is related to the length of the beam, L by means of $N=L/d$. Note that the factor N^2 accounts for the microscopic structure and the factor within the square root accounts for macroscopic properties. In the same way, the dimensionless parameters of the discrete system, α and β, can be rewritten in terms of the parameters that describe a solid continuum beam as

$$\alpha=\frac{C}{Sd^2}=\frac{EI}{\kappa GAL^2}N^2; \quad \beta=\frac{I_b}{md^2}=\frac{I}{AL^2}N^2. \tag{97}$$

As an example, we are going to study the case of a linear elastic beam with rectangular cross-section, such that

$$G=\frac{E}{2(1+\upsilon)}; \quad I=\frac{1}{12}BH^3; \quad A=BH; \quad \kappa=\frac{5}{6}, \tag{98}$$

where υ is the Poisson's ratio and B and H are the width and the height of the beam cross-section, respectively. Then, considering $\upsilon=0.3$, the parameters of Eq. (97) result

$$\alpha=\frac{1.3}{5}\lambda^2N^2; \quad \beta=\frac{1}{12}\lambda^2N^2, \tag{99}$$

Table 1
Values of the scale parameters for the continuum models.

	a_1	a_2	a_3	a_4	a_5
Classical	0	0	0	0	0
Standard I	1/4	1/2	0	0	0
Standard II	− 1/12	1/2	1/6	1/24	0
Regularization	0	0	0	0	1/6
EKE I	0	0	0	0	1/12
EKE II	0	0	0	0	1/3

which depend on the slenderness of the beam, $\lambda=H/L$. For the numerical examples, the ratio $\alpha=3\beta$ has been considered, which is representative of both rectangular ($\alpha=3.12\beta$) and circular ($\alpha=2.\widehat{8}\beta$) cross sections.

4. Treatment of edge condition

In the previous sections, dispersion relations have been obtained for both the discrete model and the proposed non-classical continuum models. In order to carry out a more exhaustive analysis of the problem, in this section we are going to study the natural frequencies in finite (bounded) solids. For this purpose, two problems are treated, a *simply-supported* beam and a *clamped-free* beam, thus dealing with the three common boundary conditions in this kind of solid: *simple support, built-in* and *free end*. It is worth mentioning that previous works on the dynamic behaviours of Timoshenko beam lattices focus on simply-supported beams, most probably because of the difficulties inherent in the consideration of clamped or free boundary conditions.

4.1. Continuum model

In this section, only non-standard models will be considered, because of the absence of higher-order derivatives in their governing equations, and of extra boundary conditions. However, these models differ from the classical Timoshenko beam model, presenting non-classical terms. For this reason the boundary conditions of the non-standard models require a different treatment. Hence, an axiomatic continuum model is proposed to obtain these new non-classical boundary conditions, which is derived from the classical potential energy given by Eq. (74) and the following non-classical kinetic energy expression

$$\overline{T}_d=\frac{1}{2}\alpha\left[\left(\frac{\partial \overline{v}}{\partial \tau}\right)^2+a_5\left(\frac{\partial^2 \overline{v}}{\partial \overline{x}\partial \tau}\right)^2\right]+\frac{1}{2}\alpha\beta\left[\left(\frac{\partial \theta}{\partial \tau}\right)^2+a_5\left(\frac{\partial^2 \theta}{\partial \overline{x}\partial \tau}\right)^2\right], \tag{100}$$

the Lagrangian of the system being defined by Eq. (22). If Hamilton's Principle is applied, we get the governing equations

$$\frac{\partial^2 \overline{v}}{\partial \overline{x}^2}-\frac{\partial \theta}{\partial \overline{x}}=\alpha\left(\frac{\partial^2 \overline{v}}{\partial \tau^2}-a_5\frac{\partial^4 \overline{v}}{\partial \overline{x}^2\partial \tau^2}\right); \tag{101}$$

$$\alpha\frac{\partial^2 \theta}{\partial \overline{x}^2}+\frac{\partial \overline{v}}{\partial \overline{x}}-\theta=\alpha\beta\left(\frac{\partial^2 \theta}{\partial \tau^2}-a_5\frac{\partial^4 \theta}{\partial \overline{x}^2\partial \tau^2}\right), \tag{102}$$

and boundary conditions

$$\overline{v}=0 \quad or \quad \frac{\partial \overline{v}}{\partial \overline{x}}-\theta+a_5\alpha\frac{\partial^3 \overline{v}}{\partial \overline{x}\partial \tau^2}=0; \tag{103}$$

$$\theta=0 \quad or \quad \frac{\partial \theta}{\partial \overline{x}}+a_5\beta\frac{\partial^3 \theta}{\partial \overline{x}\partial \tau^2}=0, \tag{104}$$

which coincide with the classical boundary conditions when $a_5=0$. Eqs. (101) and (102) are formally equivalent to the governing equations of the non-standard models, so that Eqs. (103) and (104) can be employed to impose the boundary conditions of these models by a suitable choice of the parameter a_5 (Table 1).

Introducing the solutions $\overline{v}(\overline{x},\tau)=V(\overline{x})e^{i\Omega\tau}$ and $\theta(\overline{x},\tau)=\psi(\overline{x})e^{i\Omega\tau}$ in Eqs. (101) and (102), it results in

$$\frac{\partial^2 V}{\partial \overline{x}^2}-\frac{\partial \psi}{\partial \overline{x}}=\alpha\left(-\Omega^2V+a_5\Omega^2\frac{\partial^2 V}{\partial \overline{x}^2}\right); \tag{105}$$

$$\alpha\frac{\partial^2 \psi}{\partial \overline{x}^2}+\frac{\partial V}{\partial \overline{x}}-\psi=\alpha\beta\left(-\Omega^2\psi+a_5\Omega^2\frac{\partial^2 \psi}{\partial \overline{x}^2}\right) \tag{106}$$

Then, the following expression for the rotation is achieved

$$\psi = \left(f_1 f_2 \frac{\partial^3 V}{\partial \bar{x}^3} + \left(f_2 \alpha \Omega^2 + 1\right) \frac{\partial V}{\partial \bar{x}}\right) \left(1 - \alpha \beta \Omega^2\right)^{-1}, \tag{107}$$

and the next governing equation in terms of displacement is obtained

$$\frac{\partial^4 V}{\partial \bar{x}^4} + \left(\frac{f_2 \alpha \Omega^2 + 1 - f_1 + f_1 \alpha \beta \Omega^2}{f_1 f_2}\right) \frac{\partial^2 V}{\partial \bar{x}^2} - \left(\left(1 - \alpha \beta \Omega^2\right) \frac{\alpha \Omega^2}{f_1 f_2}\right) V = 0, \tag{108}$$

where

$$f_1 = 1 - a_5 \alpha \Omega^2; \quad f_2 = \alpha - a_5 \alpha \beta \Omega^2. \tag{109}$$

Assuming $V(\bar{x}) = A e^{r\bar{x}}$ as a solution of Eq. (108), the following roots are found

$$r_1^2 = \frac{-\phi + \sqrt{\Delta}}{2}; \qquad r_2^2 = \frac{-\phi - \sqrt{\Delta}}{2}, \tag{110}$$

where

$$\Delta = \phi^2 + 4\left(1 - \alpha \beta \Omega^2\right) \frac{\alpha \Omega^2}{f_1 f_2}; \quad \phi = \frac{f_2 \alpha \Omega^2 + 1 - f_1 + f_1 \alpha \beta \Omega^2}{f_1 f_2}. \tag{111}$$

Thus, the general solution of Eq. (108) can be expressed as

$$V(\bar{x}) = A_1 e^{r_1 \bar{x}} + A_2 e^{-r_1 \bar{x}} + A_3 e^{r_2 \bar{x}} + A_4 e^{-r_2 \bar{x}}, \tag{112}$$

where A_1, A_2, A_3 and A_4 are arbitrary constants, determined by imposing two boundary conditions at each end of the solid. The expression of these boundary conditions can be obtained introducing the solutions $\bar{v}(\bar{x}, \tau) = V(\bar{x}) e^{i\Omega\tau}$ and $\theta(\bar{x}, \tau) = \psi(\bar{x}) e^{i\Omega\tau}$ in Eqs. (103) and (104), leading to

$$V = 0 \quad or \quad \left(1 - a_5 \alpha \Omega^2\right) \frac{\partial V}{\partial \bar{x}} - \psi = 0; \tag{113}$$

$$\psi = 0 \quad or \quad \frac{\partial \psi}{\partial \bar{x}} = 0, \tag{114}$$

which, employing the rotation expression given by Eq. (107), can be written in displacement terms as

$$\begin{aligned} &V = 0 \quad or \\ &\left(1 - a_5 \alpha \Omega^2\right) \frac{\partial V}{\partial \bar{x}} - \left(f_1 f_2 \frac{\partial^3 V}{\partial \bar{x}^3} + \left(f_2 \alpha \Omega^2 + 1\right) \frac{\partial V}{\partial \bar{x}}\right) \left(1 - \alpha \beta \Omega^2\right)^{-1} = 0; \end{aligned} \tag{115}$$

$$f_1 f_2 \frac{\partial^3 V}{\partial \bar{x}^3} + \left(f_2 \alpha \Omega^2 + 1\right) \frac{\partial V}{\partial \bar{x}} = 0 \qquad or \qquad f_1 f_2 \frac{\partial^4 V}{\partial \bar{x}^4} + \left(f_2 \alpha \Omega^2 + 1\right) \frac{\partial^2 V}{\partial^2 \bar{x}} = 0. \tag{116}$$

Notice that the natural boundary condition in Eq. (113) is different from that of the classical model, the latter being recovered if $a_5 = 0$. The set of Eqs. (112), (115) and (116) allow obtaining the solution for different boundary conditions, and for any of the non-standard models proposed in this paper, using the corresponding values of the parameter a_5 according to Table 1. As mentioned above, in this work the problems of simply-supported and clamped-free beams are studied, their corresponding boundary conditions being:

- Simply-supported

$$V(0) = V(N) = 0; \tag{117}$$

$$f_1 f_2 \frac{\partial^4 V}{\partial \bar{x}^4}\bigg|_{\bar{x}=0} + \left(f_2 \alpha \Omega^2 + 1\right) \frac{\partial^2 V}{\partial^2 \bar{x}}\bigg|_{\bar{x}=0} = 0; \tag{118}$$

$$f_1 f_2 \frac{\partial^4 V}{\partial \bar{x}^4}\bigg|_{\bar{x}=N} + \left(f_2 \alpha \Omega^2 + 1\right) \frac{\partial^2 V}{\partial^2 \bar{x}}\bigg|_{\bar{x}=N} = 0. \tag{119}$$

- Clamped-free

$$V(0) = 0; \tag{120}$$

$$f_1 f_2 \frac{\partial^3 V}{\partial \bar{x}^3}\bigg|_{\bar{x}=0} + \left(f_2 \alpha \Omega^2 + 1\right) \frac{\partial V}{\partial \bar{x}}\bigg|_{\bar{x}=0} = 0; \tag{121}$$

$$\left(1 - a_1 \alpha \Omega^2\right) \frac{\partial V}{\partial \bar{x}}\bigg|_{\bar{x}=N} - \frac{f_1 f_2 \frac{\partial^3 V}{\partial \bar{x}^3}\Big|_{\bar{x}=N} + \left(f_2 \alpha \Omega^2 + 1\right) \frac{\partial V}{\partial \bar{x}}\Big|_{\bar{x}=N}}{1 - \alpha \beta \Omega^2} = 0; \tag{122}$$

$$f_1 f_2 \frac{\partial^4 V}{\partial \bar{x}^4}\bigg|_{\bar{x}=N} + \left(f_2 \alpha \Omega^2 + 1\right) \frac{\partial^2 V}{\partial^2 \bar{x}}\bigg|_{\bar{x}=N} = 0. \tag{123}$$

Evaluating these boundary conditions with Eq. (112), and solving for the non-trivial solution, we can obtain the natural frequencies as a function of the number of segments N.

4.2. Discrete model

With the purpose of studying free vibrations, the displacement solution $\bar{v}_n(\tau) = V_n e^{i\Omega\tau}$ is considered. Thus, Eq. (14) leads to

$$\begin{aligned} &V_{n+2} - 4V_{n+1} + 6V_n - 4V_{n-1} + V_{n-2} \\ &+\left(\alpha + \beta\right)\left(V_{n+1} - 2V_n + V_{n-1}\right)\Omega^2 - \Omega^2 + \Omega^4 \alpha \beta V_n = 0. \end{aligned} \tag{124}$$

In this work, a general solution for the difference Eq. (124) is obtained by following a procedure applied in [67,68] for an Euler-Bernouilli beam model. For this purpose, the following solution is assumed

$$V_{n+j} = A \zeta^j, \tag{125}$$

Eq. (124) resulting in

$$\begin{aligned} &\left(\zeta + \frac{1}{\zeta}\right)^2 - 4\left(\zeta + \frac{1}{\zeta}\right) + \left(4 - \Omega^2\right) + \left(\alpha + \beta\right)\left(\zeta + \frac{1}{\zeta} - 2\right)\Omega^2 - \Omega^2 \\ &+\Omega^4 \alpha \beta = 0, \end{aligned} \tag{126}$$

which has four roots, ζ_i, $i = 1, \ldots, 4$. Then, the general solution equation for the displacement of an arbitrary particle n can be written as

$$V_n = B_1 \zeta_1^n + B_2 \zeta_2^n + B_3 \zeta_3^n + B_4 \zeta_4^n, \tag{127}$$

where B_1, B_2, B_3 and B_4 are constants, to be determined by imposing two boundary conditions at each end of the system. In order to solve the discrete model for the simply-supported and clamped-free problems, the boundary conditions for the classical Timoshenko beam theory are expanded through central differences schemes as follows [46,48]. According to this theory, rotation and displacement continuous fields are related by

$$\psi = \left(\alpha \frac{\partial^3 V}{\partial \bar{x}^3} + \left(\alpha^2 \Omega^2 + 1\right) \frac{\partial V}{\partial \bar{x}}\right) \left(1 - \alpha \beta \Omega^2\right)^{-1}, \tag{128}$$

which can be used to write the classical boundary conditions in terms of the displacement as

$$V = 0 \quad or \quad \frac{\partial^3 V}{\partial \bar{x}^3} + \Omega^2 \left(\alpha + \beta\right) \frac{\partial V}{\partial \bar{x}} = 0; \tag{129}$$

$$\alpha \frac{\partial^3 V}{\partial \bar{x}^3} + \left(\alpha^2 \Omega^2 + 1\right) \frac{\partial V}{\partial \bar{x}} = 0 \quad or \quad \alpha \frac{\partial^4 V}{\partial \bar{x}^4} + \left(\alpha^2 \Omega^2 + 1\right) \frac{\partial^2 V}{\partial^2 \bar{x}} = 0. \tag{130}$$

Finally, expanding Eqs. (129) and (130) through central differences schemes, the following boundary conditions for the discrete model are obtained

$$\begin{array}{l} V_n = 0 \quad or \\ \left(V_{n+2} - 2V_{n+1} + 2V_{n-1} - V_{n-2}\right) + \Omega^2 \left(\alpha + \beta\right) \left(V_{n+1} - V_{n-1}\right) = 0; \end{array} \tag{131}$$

$$\begin{array}{l} \alpha \left(V_{n+2} - 2V_{n+1} + 2V_{n-1} - V_{n-2}\right) + \left(\alpha^2 \Omega^2 + 1\right) \left(V_{n+1} - V_{n-1}\right) = 0 \quad or \\ \alpha \left(V_{n+2} - 4V_{n+1} + 6V_n - 4V_{n-1} + V_{n-2}\right) + \left(\alpha^2 \Omega^2 + 1\right) \left(V_{n+1} - 2V_n + V_{n-1}\right) = 0. \end{array} \tag{132}$$

Therefore, the boundary conditions employed to determine the constants A_i, $i = 1, \ldots, 4$, depending on the problem treated, are:

- Simply-supported

$$V_0 = V_N = 0; \tag{133}$$

$$\alpha \left(V_2 - 4V_1 - 4V_{-1} + V_{-2}\right) + \left(\alpha^2 \Omega^2 + 1\right) \left(V_1 + V_{-1}\right) = 0; \tag{134}$$

$$\alpha \left(V_{N+2} - 4V_{N+1} - 4V_{N-1} + V_{N-2}\right) + \left(\alpha^2 \Omega^2 + 1\right) \left(V_{N+1} + V_{N-1}\right) = 0. \tag{135}$$

- Clamped-free

$$V_0 = 0; \tag{136}$$

$$\alpha \left(V_2 - 2V_1 + 2V_{-1} - V_{-2}\right) + \left(\alpha^2 \Omega^2 + 1\right) \left(V_1 - V_{-1}\right) = 0; \tag{137}$$

$$\left(V_{N+2} - 2V_{N+1} + 2V_{N-1} - V_{N-2}\right) + \Omega^2 \left(\alpha + \beta\right) \left(V_{N+1} - V_{N-1}\right) = 0; \tag{138}$$

$$\begin{array}{l} \alpha \left(V_{N+2} - 4V_{N+1} + 6V_N - 4V_{N-1} + V_{N-2}\right) \\ \quad + \left(\alpha^2 \Omega^2 + 1\right) \left(V_{N+1} - 2V_N + V_{N-1}\right) = 0. \end{array} \tag{139}$$

Evaluating these boundary conditions with Eq. (127), and solving for the non-trivial solution, the natural frequencies can be obtained for each problem as a function of the number of segments N. Note how the previous equations make use of four virtual particles, with indices $n = -1$ and $n = -2$ at the left end and $n = N + 1$ and $n = N + 2$ at the right one. The displacement of these particles can be evaluated, in the same way as the other particles appearing in the boundary condition equations, with Eq. (127). The treatment of edge conditions involving virtual particles is rather common in this kind of problem, such as is proposed in works by Challamel et al. [42,68] and Wang et al. [46].

5. Analysis of bending and shear spectra

As it has been observed in Section 2, there are two different spectra in the wave propagation through Timoshenko beam lattices. This phenomenon has been thoroughly studied by Cazzani et al. [69,70] for the Classical Timoshenko beam theory, and is going to be studied for non-classical continuum models in this section, since it is connected to a critical frequency that marks the transition between bending-dominated to shear-dominated defirmation modes. For this purpose, points in the dispersion curves of the non-standard models are going to be related to the corresponding wavenumbers and frequencies of the natural modes in the simply-supported configuration. Moreover, the analysis shows that the size-effects modifies the value of this transition frequency through the number of segments N (consequently through the characteristic length of the lattice d). Discrete and Classical models will also be analysed for comparison.

5.1. Transition frequency

When solving Eq. (108), a transition frequency can be found from the roots in Eq. (110). This frequency is given by the expression

$$\Omega_{trans} = \frac{1}{\sqrt{\alpha\beta}}, \tag{140}$$

which coincides with the limiting frequency in the long-wave range ($\overline{K} = 0$) for the shear spectrum, valid for all continuum models. It is worth to highlight that the dispersion relation of the discrete model, Eq. (16), also shows the same transition value (supporting the validity of the continualization). This means that natural frequencies lower than Ω_{trans} strictly correspond to bending vibration modes, shear modes appearing only for certain frequencies higher than Ω_{trans}. It should be pointed out that in some cases there is a range with mixed bending and shear frequencies, as it is explained further below. Bearing in mind Eq. (99), it can be observed how Ω_{trans} depends on N, its value decreasing when N increases.

After performing a vibration analysis of the simply-supported beam problem, it can be concluded that, for this configuration, the vibration shapes corresponding to bending are given by (considering unit amplitude)

$$V(\bar{x}) = \sin(r_2 \bar{x}) \tag{141}$$

For shear modes, the same expression is valid in the frequency range where bending modes do not appear, while the expression

$$V(\bar{x}) = \sin(r_1 \bar{x}), \tag{142}$$

should be used in the frequency range where both shear and bending modes appear intermixed. These general expressions are valid for all non-standard and Classical models, by a suitable choice of the value of a_5 in Table 1, since this scale parameter appears implicitly in r_1 and r_2, Eq. (110). In addition, it has been verified, in all the cases analysed, that the vibration shapes of the discrete model perfectly match these functions.

5.2. Influence of the transition frequency

Since Eqs. (141) and (142) are harmonic functions, the natural frequencies (bounded solids) of each model can be related to their respective dispersion curves (infinite solids). In Figs. 4 and 5, the dispersion curves and natural frequencies of the Classical and EKE I (the analysis is equally valid for the rest of the non-standard models) models are shown, considering slenderness ratio of $\lambda = 1/6$ and $N = 5$ in the first one, and $\lambda = 1/2$ and $N = 7$ in the second. The wavenumbers for each natural frequency are calculated from the wavelength of the respective shape solutions, given by Eqs. (141) and (142). These figures prove how natural frequencies match accurately with the dispersion curves, demonstrating how when $\Omega < \Omega_{trans}$ only bending vibration modes appear, whereas for $\Omega > \Omega_{trans}$ both bending and shear vibration modes may arise.

The occurrence of both bending and shear modes, or shear-only modes, above the transition frequency depends on λ and N, as well as on the considered model. For instance, for the Classical model both kinds of deformation modes appear intermixed above Ω_{trans}, as it is shown in Figs. 4 and 5, since both dispersion spectra monotonically increase with $\overline{K}$ (for a detailed analysis of this phenomenon in the

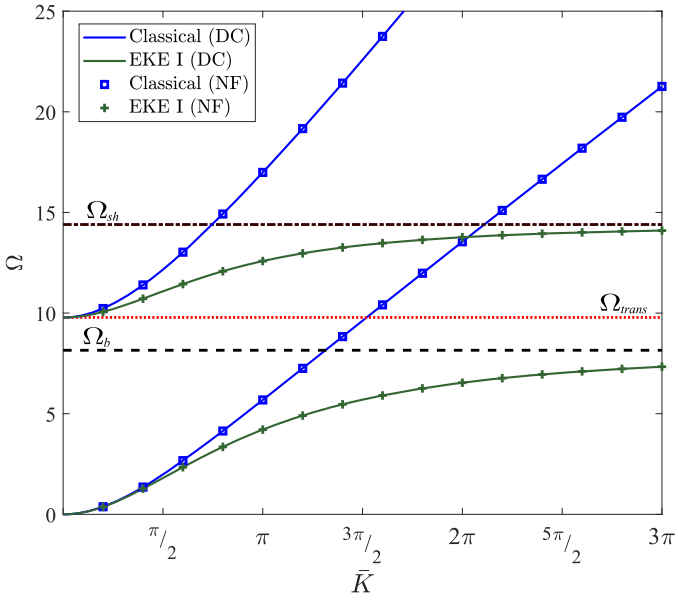

Fig. 4. Correlation between dispersion curves (DC) and natural frequencies (NF) of a simply-supported beam. Comparison of bending and shear spectra of the Classical and EKE I models, with a slenderness ratio of $\lambda = 1/6$ and $N = 5$. Situation in which $\Omega_{trans} > \Omega_b$.

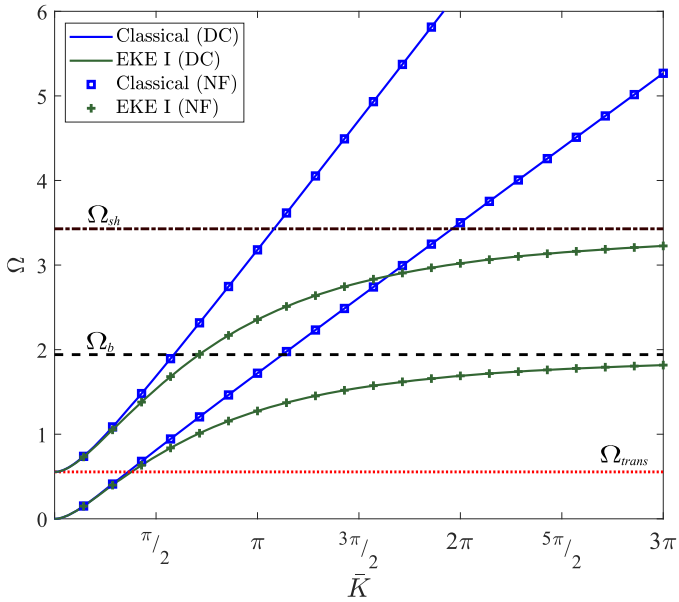

Fig. 5. Correlation between dispersion curves (DC) and natural frequencies (NF) of a simply-supported beam. Comparison of bending and shear spectra of the Classical and EKE I models, with a slenderness ratio of $\lambda = 1/2$ and $N = 7$. Situation in which $\Omega_{trans} < \Omega_b$.

Classical Timoshenko beam, see [69,70]). Nevertheless, the dispersion curves of non-standard models tend to constant values when $\bar{K} \to \infty$, which are given by

$$\Omega_{sh} = \sqrt{\frac{a_5\left(\alpha+\beta\right) + \sqrt{a_5^2(\alpha-\beta)^2}}{2a_5^2\alpha\beta}}; \quad \Omega_b = \sqrt{\frac{a_5\left(\alpha+\beta\right) - \sqrt{a_5^2(\alpha-\beta)^2}}{2a_5^2\alpha\beta}}, \tag{143}$$

where subindices *sh* and *b* in Ω refer to shear and bending, respectively. For this reason, two different scenarios are possible, depending on the values of α, β and on the model considered (scale parameter a_5). For instance, Fig. 4 illustrates a case where $\Omega_{trans} > \Omega_b$, so only shear vibration modes appear for frequencies higher than Ω_{trans}. However, Fig. 5 shows a case with a higher slenderness ratio and a higher value of N (lower value of Ω_{trans}), leading to the situation in which $\Omega_{trans} < \Omega_b$, thus presenting a range, $\Omega_{trans} < \Omega < \Omega_b$, in which bending and shear vibration modes are mixed.

Bearing in mind that the non-standard continuum models developed are intended to capture the behaviour of the discrete model, and that the dispersion relation of the latter is of interest exclusively in the IBZ (because of its periodicity properties described in Section 2), it is convenient to limit the study of frequencies and their comparison for discrete and continuum models to the range of $0 < \bar{K} < \pi$. Fig. 6 shows the case with $\lambda = 1/2$ and $N = 7$ in the IBZ and appending the results of the discrete model, for which N bending and N shear modes are observed, and whose frequencies are also mixed beyond the transition value Ω_{trans}. Note that each Nth mode is at the limit of the IBZ for the corresponding branch. For a suitable comparison with the frequencies of the continuum models, bending and shear modes beyond the wavenumber $\bar{K} = \pi$ must be disregarded, resulting in a consistent prediction of both bending and shear frequencies with the non-standard model, much better than that obtained with the Classical one.

6. Discussion

In this section, the dynamic behaviour of the continuum models proposed in this work will be assessed in two different ways, in both of them evaluating their suitability to capture the performance of the discrete model, considered as a reference. Firstly, the dispersion curves of the models will be presented, and subsequently, the natural frequencies obtained by following the resolution method set out in Section 4 will be compared.

6.1. Dispersion analysis

The dispersion curves corresponding to the different continuum models are presented in Fig. 7, together with that of the discrete model, considering $\alpha = 0.15$ and $\beta = \alpha/3$. In addition, the relative errors of these curves are plotted in Fig. 8, in order to assess their accuracy in fitting the discrete model. This error is defined as

$$Error(\%) = \frac{|\Omega_{continuum} - \Omega_{discrete}|}{\Omega_{discrete}} \times 100. \tag{144}$$

As mentioned in the Section 2, there are two sets of curves for all models, one corresponding to the propagation of bending waves, which tends to zero for long wavelengths, and another corresponding to the propagation of shear waves, which tends to $(\alpha\beta)^{-0.5}$ when $\bar{K} \to 0$. In both sets, for long wavelengths, the curves of the continuum models show similar behaviour, fitting successfully to that of the discrete model. This does not occur when the wavenumber increases, as each model then behaves in a different way, size-effects playing a significant role. Relative errors corresponding to the propagation of bending waves are plotted in Fig. 8(b), where it can be seen how the Regularization model shows the best performance, with errors lower than 8% for $\bar{K} < 3\pi/4$ and around 20% in the limit of the IBZ. Nevertheless, this is not the case for the propagation of shear waves, whose relative error is shown in Fig. 8(a), the Standard II model showing the best performance, with errors lower than 5% for $\bar{K} < 3\pi/4$ and close to 10% in the limit of the IBZ. For this reason, it is not easy to determine the most suitable continuum model by analysing only the dispersion curves, since their fit to those of the discrete model depends on the value of α and β, which are function of λ and N, as it can be seen in Eq. (99).

In addition, it is worth carrying out a deeper analysis of these models, looking for possible physical inconsistencies. This is the case of the Standard II model, which provides imaginary frequencies for high wavenumbers. This fact implies an exponential growth of short waves,

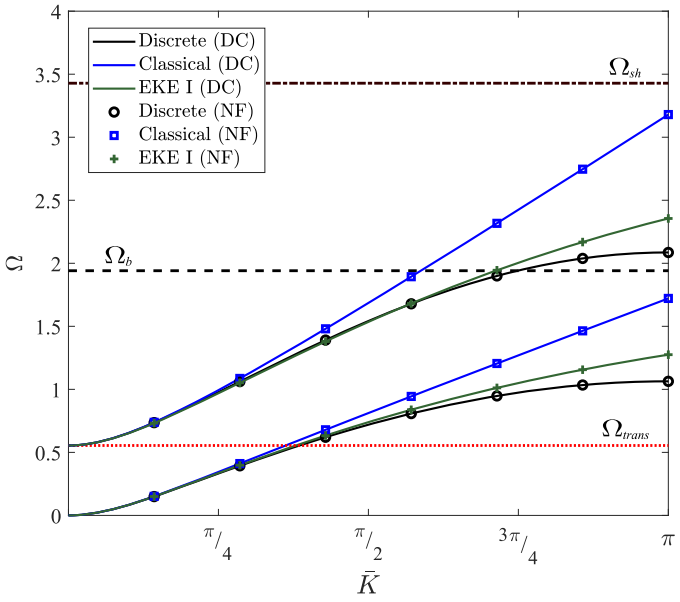

Fig. 6. Correlation between dispersion curves (DC) and natural frequencies (NF) of a simply-supported beam. Comparison of bending and shear spectra of the Classical and EKE I models with those of the Discrete one (considered as a reference), with a slenderness ratio of $\lambda = 1/2$ and $N = 7$. Situation in which $\Omega_{trans} < \Omega_b$.

which has no sense in a conservative model with no external energy source (see [71] for more details on this issue in a 1D rod lattice). On the other hand, we examine the existence of limits on the velocity at which the perturbations can be propagated [41,71]. For this purpose, we evaluate whether the group velocity of all the models (both bending and shear waves), $\bar{v}_g = \partial\Omega/\partial\bar{K}$, is bounded, concluding that for the standard models, the velocity is not limited, since its group velocity tends to infinity when $\bar{K}\to\infty$. However, this drawback disappears for the non-standard models, including in their governing equations the scaling parameter a_5, which increases the compliance of the model. It should be noted that the group velocity of all models presents the same trend

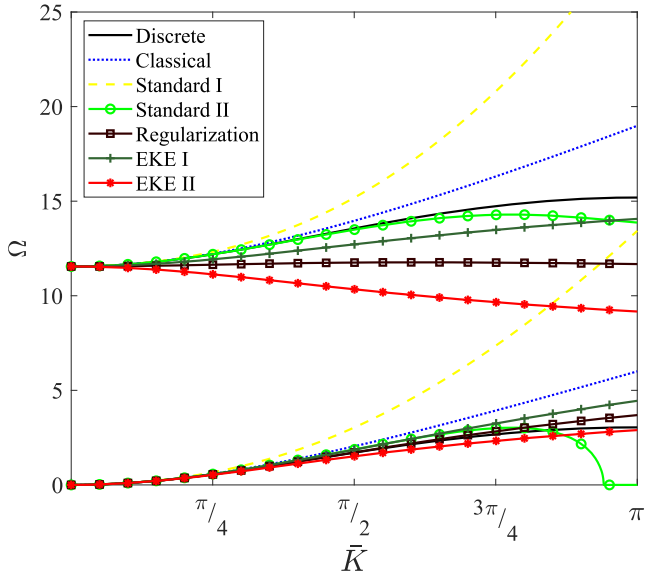

Fig. 7. Dispersion curves, relating dimensionless frequencies Ω and dimensionless wavenumber $\bar{K}$, for $\alpha = 0.15$ and $\beta = \alpha/3$. Comparison of the continuum models with the discrete one (considered as a reference). Representation of both bending (bottom curves) and shear (top curves) spectra within the IBZ.

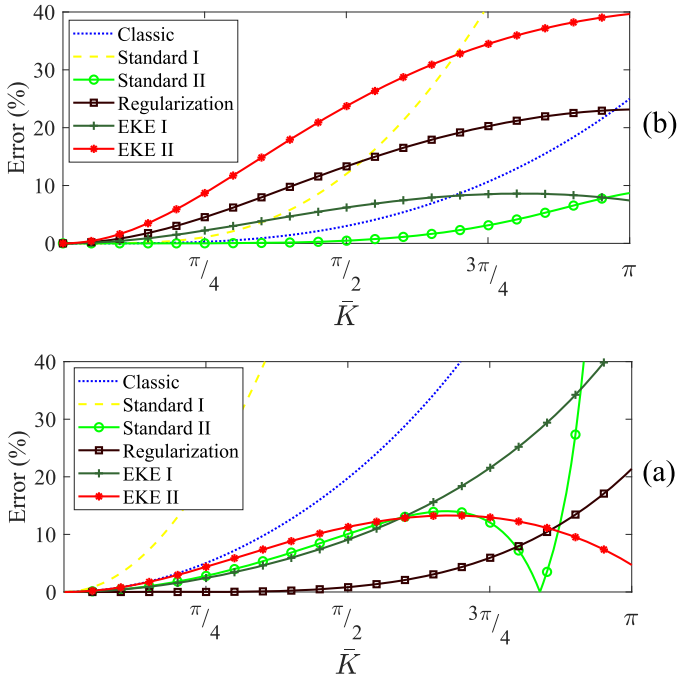

Fig. 8. Relative error of the dispersion curves (within the IBZ) for $\alpha = 0.15$ and $\beta = \alpha/3$, considering the discrete model as a reference. (a) Propagation of bending waves. (b) Propagation of shear waves.

regardless of whether bending or shear wave propagation is involved.

6.2. Natural frequencies

Dispersion analysis is a key method to uncover the dynamic behaviour of the models. However, we have seen that in the Timoshenko beam problem, which involves the propagation of two kinds of waves, it is difficult to conclude which continuum model is more suitable to capture the performance of the discrete model. Furthermore, as previously mentioned, solids have finite dimensions in real applications, and are affected by the boundary conditions imposed to them. Therefore, in this section we are going to analyse the results for finite solids, developed in Section 4. Firstly, we will study the cases with $\lambda = 1/4$ and $\lambda = 1/10$ for which $\Omega_{trans} > \Omega_b$, shear vibration modes showing high frequencies, far above the bending ones. For this reason, the dimensional natural frequencies, Eq. (96), for the first four bending modes of the simply-supported and clamped-free beam problems are going to be plotted, considering $EI/(\rho AL^4) = 1$. Lastly, as an illustrative example, natural shear frequencies will be shown for a case with $\lambda = 1/2$, where $\Omega_{trans} < \Omega_b$, shear modes starting at lower values. Continuum models are compared with the discrete one, representing their natural frequencies as a function of N. The standard models are not considered here because of the inconsistencies found in the dispersion analysis and the need for extra boundary conditions.

6.2.1. Simply-supported beam (bending vibration modes)

Figs. 9 and 10 show the dimensional natural frequencies of the simply-supported problem for the first four modes, considering $\lambda = 1/4$ and $\lambda = 1/10$, respectively.

As it can be seen, all non-classical models provide similar values of frequencies for large N, dropping the dependence on it, and coinciding with the length-scale free Classical model. If the total length of the beam is kept constant, the straight segment length, d, reduces as the number of them, N, rises, thus minimising the influence of size-effects. However, for low values of N, the behaviour of all the non-classical models differs from that of the Classical one, showing distinct behaviours. Moreover, it can be easily proven that all models tend to the corresponding Euler-

Bernouilli ones when the slenderness ratio, λ, tends to zero (see [48] to compare with the frequencies of Euler-Bernoulli models).

To assess the accuracy of the continuous models in capturing the behaviour of the discrete model, the relative errors for $\lambda = 1/4$ and $\lambda = 1/10$ have been plotted in Figs. 11 and 12, respectively.

Analysing Fig. 11 ($\lambda = 1/4$), it can be observed that for all models, with the exception of the EKE II model, the error increases for high modes. The Regularization model shows the best performance, its maximum errors being lower than 3% for the first three modes, increasing to around 15% for the fourth when $N = 4$. Notice that in this case, the fourth mode shape is given by a harmonic function with a wavelength of $2d$ (equivalent to $\overline{K} = \pi$), which corresponds to the limit of the IBZ [72]. Interestingly, the EKE II model, which shows the worst performance for the first modes, improves its performance in the limit of the IBZ, consistently with the trend observed in the relative errors of the bending dispersion curve, Fig. 8(b). In order to further analyse this behaviour, Fig. 13 shows the relative error of the bending dispersive curves of the different models in the limit of the IBZ, for several values of α, and $\beta = \alpha/3$, proving that the EKE II model is the one that provides the best performance in this zone. Observing Fig. 12 ($\lambda = 1/10$), it can be seen how all the models increase their error (with respect to the those shown for the $\lambda = 1/4$ case), except the EKE II model, which decreases, showing a maximum relative error of around 10% for modes 2, 3 and 4 (close to the limit of the IBZ). Nonetheless, the Regularization model shows the best performance for the first modes, with errors less than 0.3% and 3% for the first and second modes, respectively.

6.2.2. *Clamped-free beam (bending vibration modes)*

The dimensional natural frequencies of the clamped-free problem for the first four modes are plotted in Figs. 14 and 15, considering $\lambda = 1/4$ and $\lambda = 1/10$, respectively.

As in the simply-supported beam problem, it can be proven how for high values of N, the frequencies of all the non-classical models coincide with those of the Classical one, losing the length-scale influence. In the same way, non-classical models show unequal performances for low values of N, differing from the Classical model, and it can be easily proven how they tend to the corresponding Euler-Bernouilli models when the slenderness ratio of the beam (λ) tends to zero. Again, to further test the ability of the continuum models to capture the behaviour

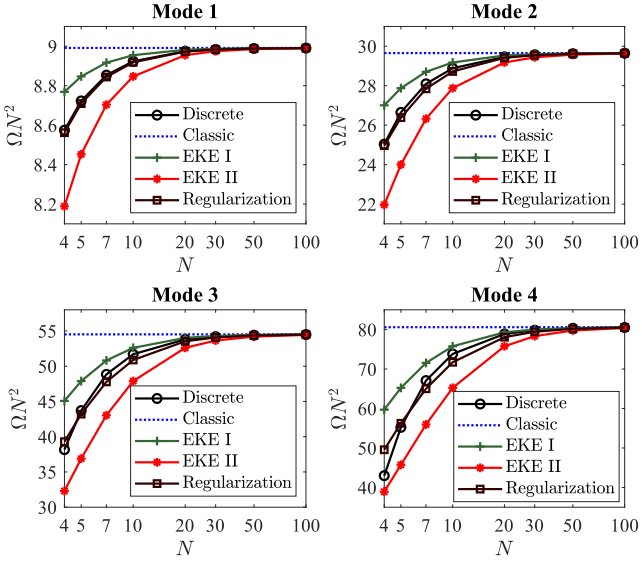

Fig. 9. Dimensional bending natural frequencies of simply-supported beam with slenderness ratio $\lambda = 1/4$ as a function of the number of segments N. Comparison of the low-order continuum models with the discrete one (considered as a reference), and the Classical Timoshenko continuum model (length-scale free). Representation of the first four modes.

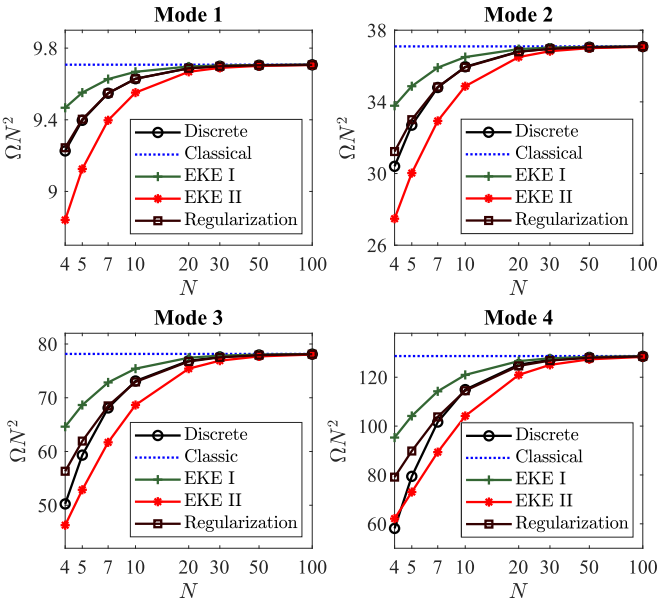

Fig. 10. Dimensional bending natural frequencies of simply-supported beam with slenderness ratio $\lambda = 1/10$ as a function of the number of segments N. Comparison of the low-order continuum models with the discrete one (considered as a reference), and the Classical Timoshenko continuum model (length-scale free). Representation of the first four modes.

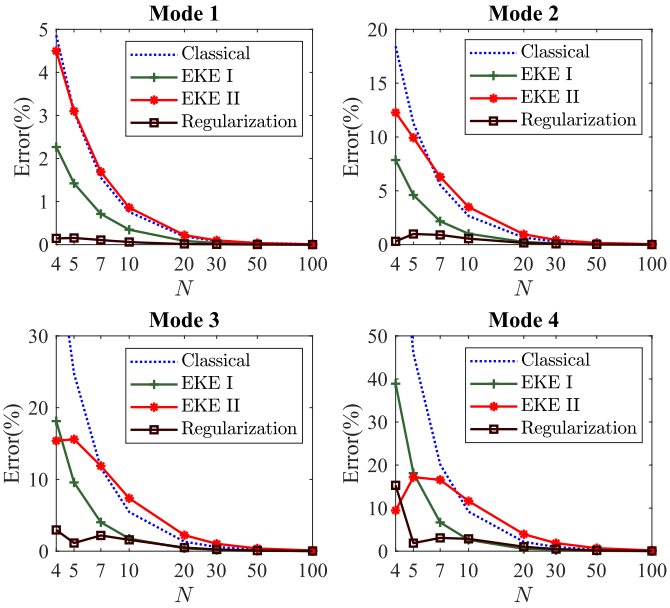

Fig. 11. Relative error of dimensional bending natural frequencies of simply-supported beam with slenderness ratio $\lambda = 1/4$ as a function of the number of segments N. Comparison between the low-order continuum models and the Classical Timoshenko continuum model (length-scale free). Representation of the first four modes.

of the discrete model, the relative errors of the clamped-free beam for $\lambda = 1/4$ and $\lambda = 1/10$ are shown in Figs. 16 and 17, respectively.

Fig. 16 ($\lambda = 1/4$) shows how all models increase their error for higher modes, EKE II and Regularization models showing the best performance. EKE II model presents the lowest error in the first mode, its maximum value being lower than 0.5%, while in the second mode its error is similar to that of the Regularization model, and in the modes three and four the Regularization model exhibits the lowest error, being lower than 10% in mode 4. On the other hand, for the case $\lambda = 1/10$

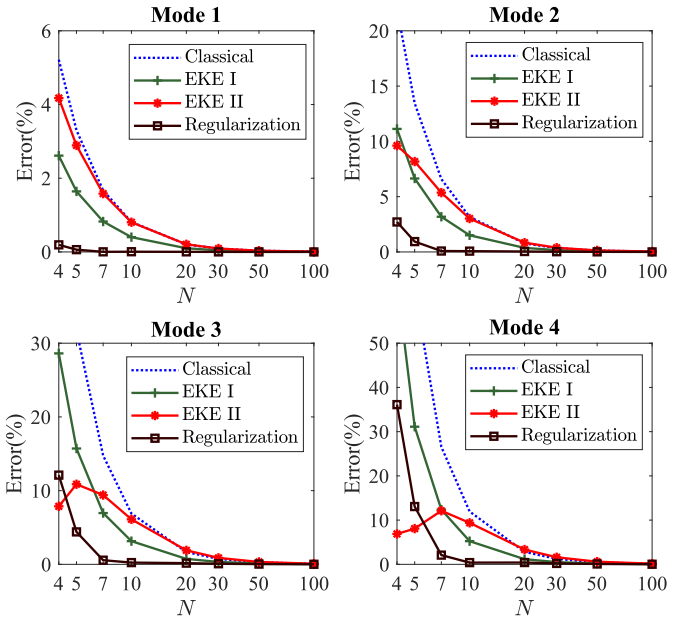

Fig. 12. Relative error of dimensional bending natural frequencies of simply-supported beam with slenderness ratio $\lambda = 1/10$ as a function of the number of segments N. Comparison between the low-order continuum models and the Classical Timoshenko continuum model (length-scale free). Representation of the first four modes.

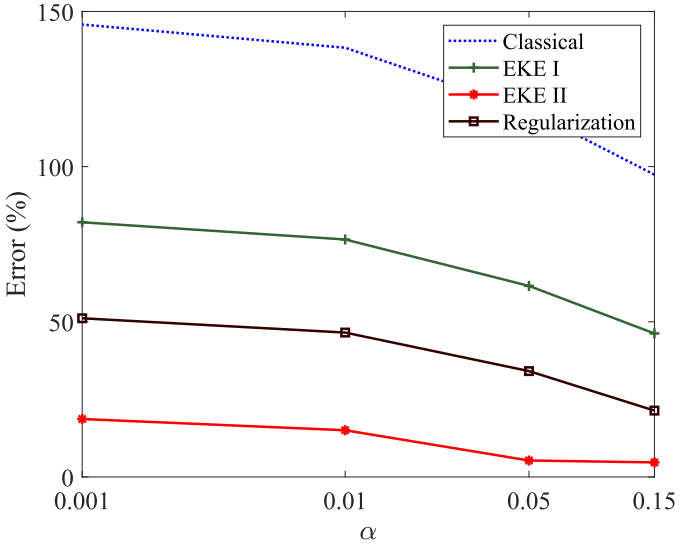

Fig. 13. Relative error of the bending dispersion curves in the limit of the IBZ (corresponding to mode 4 and $N = 4$), for different values of α, and $\beta = \alpha/3$. Comparison between the low-order continuum models and the Classical Timoshenko continuum model.

(Fig. 17), the relative error of all models, with the exception of the EKE II model, increases with respect to the case $\lambda = 1/4$. EKE II model shows the best performance for low values of N in all modes, its maximum error being lower than 10% and presenting very low error at the limit of the IBZ (mode 4 and $N = 4$).

6.2.3. Simply-supported beam (shear vibration modes)

Now, a simply-supported beam with slenderness ratio $\lambda = 1/2$ is considered, for which $\Omega_{trans} < \Omega_b$, so shear and bending modes are mixed for frequencies higher than the transition one. Figs. 18 and 19 show the first four shear modes and the relative errors, respectively. It can be observed that all non-standard models behave as in the cases studied previously, matching the Classical one when N increases (loss of length-scale influence), and differing from each other for low values of N. However, in this case, the EKE I model is the one that shows the best performance, with errors lower than 2% in the first three modes and close to 10% for the fourth one (limit of the IBZ).

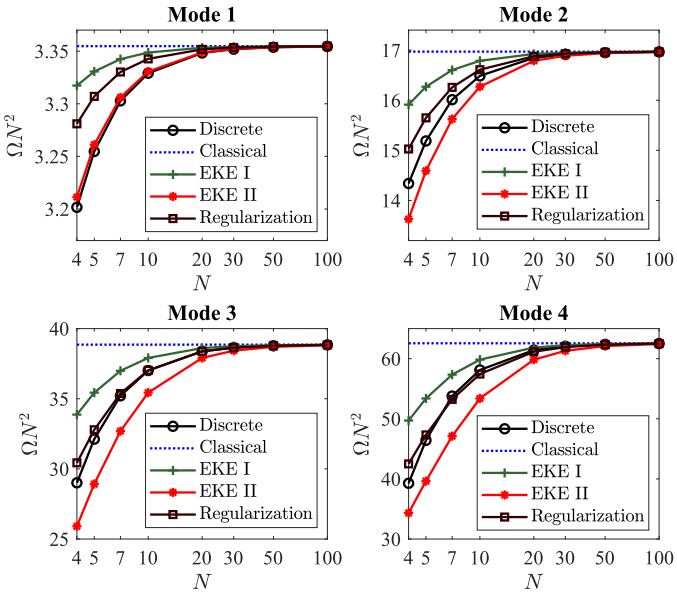

Fig. 14. Dimensional bending natural frequencies of clamped-free beam with slenderness ratio $\lambda = 1/4$ as a function of the number of segments N. Comparison of the low-order continuum models with the discrete one (considered as a reference), and the Classical Timoshenko continuum model (length-scale free). Representation of the first four modes.

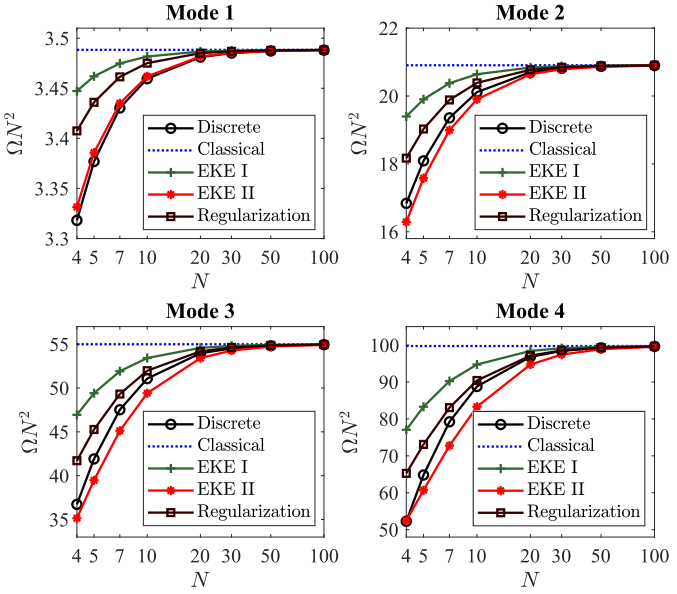

Fig. 15. Dimensional bending natural frequencies of clamped-free beam with slenderness ratio $\lambda = 1/10$ as a function of the number of segments N. Comparison of the low-order continuum models with the discrete one (considered as a reference), and the Classical Timoshenko continuum model (length-scale free). Representation of the first four modes.

Accordingly, after evaluating the accuracy in capturing the behaviour of the discrete model and in view of their physical consistency, the non-standard models can be considered as a suitable continuous approach when describing wave propagation through a linear 1D Timoshenko bending system. Interestingly, the governing equations of these models do not require extra boundary conditions to be solved when treating finite solids.

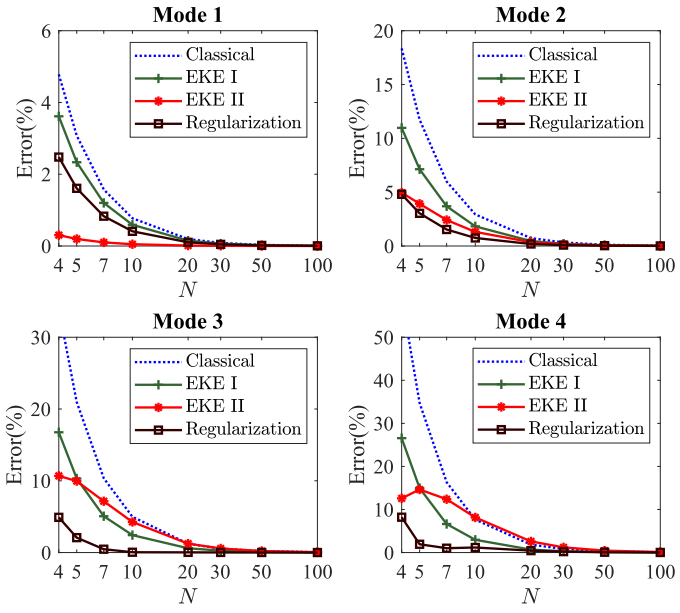

Fig. 16. Relative error of dimensional bending natural frequencies of clamped-free beam with slenderness ratio $\lambda = 1/10$ as a function of the number of segments N. Comparison between the low-order continuum models and the Classical Timoshenko continuum model (length-scale free). Representation of the first four modes.

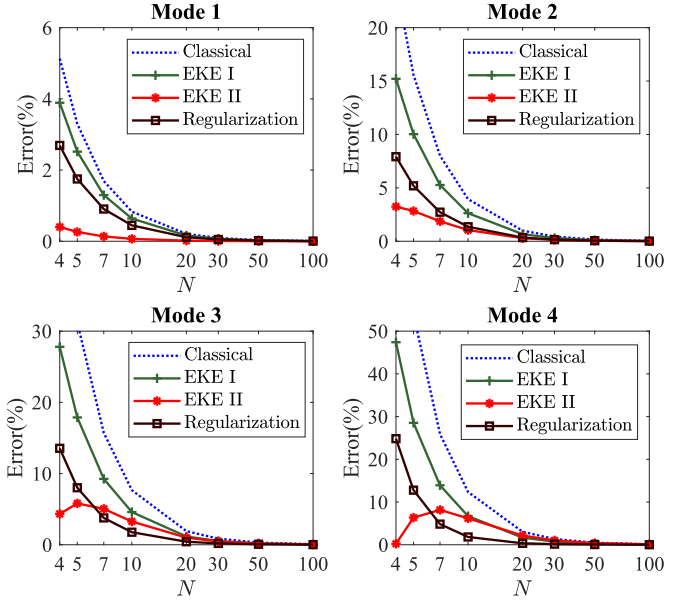

Fig. 17. Relative error of dimensional bending natural frequencies of clamped-free beam with slenderness ratio $\lambda = 1/10$ as a function of the number of segments N. Comparison between the low-order continuum models and the Classical Timoshenko continuum model (length-scale free). Representation of the first four modes.

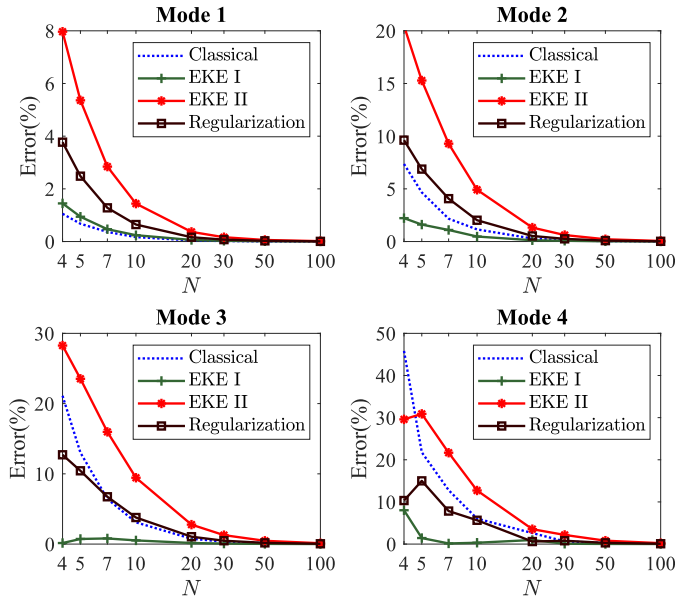

Fig. 18. Dimensional shear natural frequencies of simply-supported beam with slenderness ratio $\lambda = 1/2$ as a function of the number of segments N. Comparison of the low-order continuum models with the discrete one (considered as a reference), and the Classical Timoshenko continuum model (length-scale free). Representation of the first four modes.

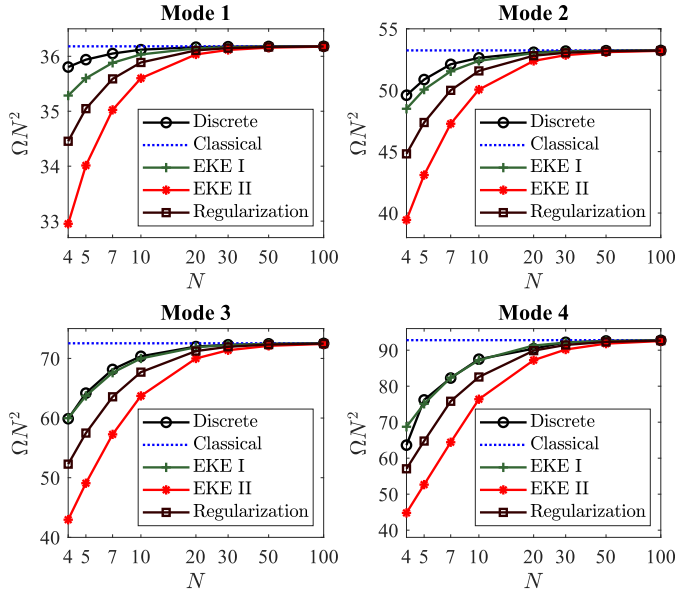

Fig. 19. Relative error of dimensional shear natural frequencies of simply-supported beam with slenderness ratio $\lambda = 1/2$ as a function of the number of segments N. Comparison between the low-order continuum models and the Classical Timoshenko continuum model (length-scale free). Representation of the first four modes.

7. Conclusions

The main target of this work is to obtain low-order non-classical continuum models, capable of capturing the dynamic behaviour of a Timoshenko discrete system as accurately as possible. For this purpose, different standard and non-standard continualization methods are applied to the discrete model and the accuracy of the new continuum models is evaluated by comparing their dispersion curves with those of the discrete model. A treatment of the edge conditions is also carried out, contrasting the natural frequencies of the non-standard models with those of the discrete one, for the simply-supported and clamped-free configurations, considering different slenderness. In addition, an analysis of the physical consistency of the achieved continuum models is performed. The following conclusions have been reached:

- The continualization of the uncoupled discrete governing equation leads to a continuous equation that cannot be derived by uncoupling

the set of two continuum governing equations, those being obtained by continualization techniques. For this reason, the uncoupled discrete governing equation should not be used as a starting point to derive continuum models, neither employing standard nor non-standard methods.

- The Standard models including size-effects present higher-order governing equations, so they need extra boundary conditions to be solved when finite solids are treated. In addition, they present some physical inconsistencies, the Standard I model showing a unbounded velocity of propagation, and the Standard II model providing imaginary frequencies for high wavenumbers, which means an exponential growth of short waves, making no sense in a conservative model with no external energy sources.
- These drawbacks are eliminated by employing the proposed non-standard continualization methods. These methods have been applied here for the first time to the kind of lattice studied in this work, and lead to physically consistent models that present governing equations with space-time derivatives that capture the size-effects, while keeping their low order. All non-standard models proposed in this paper are formally equivalent, the difference being in the value of the scale factor a_5 of these derivatives.
- There is a transition frequency Ω_{trans}, above which shear modes appear, which depends on the slenderness ratio λ and on the value of N. Two situations can arise, according the value of the asymptote Ω_b to which the bending dispersion curves of non-standard models tend in the short-wave limit. If $\Omega_{trans} > \Omega_b$, both kinds of modes are completely separate. However, if $\Omega_{trans} < \Omega_b$, there is a range $\Omega_{trans} < \Omega < \Omega_b$ in which these two kinds of vibration modes are mixed.
- The discrete model presents $2N$ (freedom degrees of the system) modes, one half in bending and the other half in shear modes. Consequently, each Nth mode is at the limit of the IBZ for the corresponding branch. After comparing natural frequencies, it is concluded that the relative error of all models increases for high modes, the EKE II and Regularization models showing the best performance in both simply-supported and clamped-free problems, when bending modes are studied. Furthermore, it has been observed that all models except the EKE II one increase their error for slender beams (i.e. as the slenderness ratio, λ, decreases). Interestingly, the EKE II model presents low errors at the limit of the IBZ. On the other hand, it has been found that the EKE I model shows the best performance when shear modes of a simply-supported beam are studied.

In brief, this paper presents a comprehensive study on the application of continualization methods in order to develop non-classical continuum models capable of capturing the dispersive behaviour of a Timoshenko beam lattice. Non-standard models show appropriate performances, besides being physically consistent and not requiring extra boundary conditions to be solved. For these reasons, these continuum models are regarded as a suitable approach to describe wave propagation in this kind of system.

Declaration of Competing Interest

The authors declare that they have no known competing financial interests or personal relationships that could have appeared to influence the work reported in this paper.

Acknowledgements

The authors acknowledge support from MCIN/ AEI /10.13039/501100011033 under Grants numbers PGC2018-098218-B-I00 and PRE2019-088002. FEDER: A way to make Europe. ESF invests in your future.

Appendix A. Derivation of enriched kinetic energy densities

In this work, two different enriched kinetic energy models (EKE I and EKE II) are proposed. In these models, the first spatial derivative is expanded through a progressive and a central differences scheme, given by Eqs. (68) and (50) respectively, leading to the general expression presented below, which relates both continuous and discrete variables

$$Y_n = Q_i Y; \quad Y = \overline{v}, \theta; \quad i = 1, 2, \tag{A.1}$$

where indices 1 and 2 refer to EKE I and EKE II models, and Q_1 and Q_2 are given by Eqs. (72) and (80), respectively. Employing Eq. (A.1), the kinetic energy of the discrete system can be continualized as

$$\overline{T}_i = \frac{1}{2}\sum_n \left[\alpha\left(\frac{\partial \overline{v}_n}{\partial \tau}\right)^2 + \alpha\beta\left(\frac{\partial \theta_n}{\partial \tau}\right)^2\right] = \frac{1}{2}\int_L \left[\alpha \frac{\partial \overline{v}}{\partial \tau} Q_i \frac{\partial \overline{v}}{\partial \tau} + \alpha\beta\left(Q_i \frac{\partial \theta}{\partial \tau} Q_i \frac{\partial \theta}{\partial \tau}\right)\right] d\overline{x} = \frac{1}{2}\int_L \left[\alpha \frac{\partial \overline{v}}{\partial \tau} Q_i^* Q_i \frac{\partial \overline{v}}{\partial \tau} + \alpha\beta\left(\frac{\partial \theta}{\partial \tau} Q_i^* Q_i \frac{\partial \theta}{\partial \tau}\right)\right] d\overline{x}, \tag{A.2}$$

where $Q_i^* = Q_i(-\partial_{\overline{x}})$ is the adjoint operator of Q_i. Hence, for EKE I and EKE II models,

$$Q_1^* Q_1 = 1 - \frac{1}{12}\partial_{\overline{x}}^2 + O(\partial_{\overline{x}}^4), \tag{A.3}$$

and

$$Q_2^* Q_2 = 1 - \frac{1}{3}\partial_{\overline{x}}^2 + O(\partial_{\overline{x}}^4), \tag{A.4}$$

respectively. Now, Eq. (A.2) is integrated by parts, leading to

$$\overline{T}_1 = \frac{1}{2}\int_0^N \left[\alpha\left(\frac{\partial \overline{v}}{\partial \tau}\right)^2 + \frac{\alpha}{12}\left(\frac{\partial^2 \overline{v}}{\partial \overline{x}\partial \tau}\right)^2 + \alpha\beta\left(\frac{\partial \theta}{\partial \tau}\right)^2 + \frac{\alpha\beta}{12}\left(\frac{\partial^2 \theta}{\partial \overline{x}\partial \tau}\right)^2\right] d\overline{x} - \frac{\alpha}{12}\frac{\partial \overline{v}}{\partial \tau}\frac{\partial^2 \overline{v}}{\partial \overline{x}\partial \tau}\Big|_0^N - \frac{\alpha\beta}{12}\frac{\partial \theta}{\partial \tau}\frac{\partial^2 \theta}{\partial \overline{x}\partial \tau}\Big|_0^N; \tag{A.5}$$

$$\overline{T}_2 = \frac{1}{2}\int_0^N \left[\alpha\left(\frac{\partial \overline{v}}{\partial \tau}\right)^2 + \frac{\alpha}{3}\left(\frac{\partial^2 \overline{v}}{\partial \overline{x}\partial \tau}\right)^2 + \alpha\beta\left(\frac{\partial \theta}{\partial \tau}\right)^2 + \frac{\alpha\beta}{3}\left(\frac{\partial^2 \theta}{\partial \overline{x}\partial \tau}\right)^2\right] d\overline{x} - \frac{\alpha}{3}\frac{\partial \overline{v}}{\partial \tau}\frac{\partial^2 \overline{v}}{\partial \overline{x}\partial \tau}\Big|_0^N - \frac{\alpha\beta}{3}\frac{\partial \theta}{\partial \tau}\frac{\partial^2 \theta}{\partial \overline{x}\partial \tau}\Big|_0^N, \tag{A.6}$$

which correspond to the EKE I and EKE II models, respectively. Considering that the boundary terms of Eqs. (A.5) and (A.6) do not play any role in the govering equation when applying Hamilton's principle, the following expressions can be assumed for each enriched kinetic energy density

$$\overline{T}_{d,1} = \frac{1}{2}\left[\left(\frac{\partial \overline{v}}{\partial \tau}\right)^2 + \frac{1}{12}\left(\frac{\partial^2 \overline{v}}{\partial \overline{x}\partial \tau}\right)^2 + \beta\left(\frac{\partial \theta}{\partial \tau}\right)^2 + \frac{\beta}{12}\left(\frac{\partial^2 \theta}{\partial \overline{x}\partial \tau}\right)^2\right]; \tag{A.7}$$

$$\overline{T}_{d,1} = \frac{1}{2}\left[\left(\frac{\partial \overline{v}}{\partial \tau}\right)^2 + \frac{1}{3}\left(\frac{\partial^2 \overline{v}}{\partial \overline{x}\partial \tau}\right)^2 + \beta\left(\frac{\partial \theta}{\partial \tau}\right)^2 + \frac{\beta}{3}\left(\frac{\partial^2 \theta}{\partial \overline{x}\partial \tau}\right)^2\right], \tag{A.8}$$

both being positive definite.

References

[1] Zhang Y, Wei Q. The role of nanomaterials in electroanalytical biosensors: a mini review. J Electroanal Chem 2016;781:401–9.
[2] Oh J-W, Jung J-Y, Kim H-W, Hong S, Sung K-Y, Bae D-S. Gap size effect on the tribological characteristics of the roller for deep-sea mining robot. Mar Georesour Geotechnol 2017;35:120–6.
[3] Esfahani S, Khadem SE, Mamaghani AE. Nonlinear vibration analysis of an electrostatic functionally graded nano-resonator with surface effects based on nonlocal strain gradient theory. Int J Mech Sci 2019;151:508–22.
[4] Yin YM, Li HY, Xu J, Zhang C, Liang F, Li X, et al. Facile fabrication of flexible pressure sensor with programmable lattice structure. ACS Appl Mater Interfaces 2021;13:10388–96.
[5] Eom K, Park HS, Yoon DS, Kwon T. Nanomechanical resonators and their applications in biological/chemical detection: nanomechanics principles. Phys Rep 2011;503:115–63.
[6] Caldas EM, Novatzky D, Deon M, de Menezes EW, Hertz PF, Costa TMH, et al. Pore size effect in the amount of immobilized enzyme for manufacturing carbon ceramic biosensor. Microporous Mesoporous Mater 2017;247:95–102.
[7] Habibi M, Hashemabadi D, Safarpour H. Vibration analysis of a high-speed rotating GPLRC nanostructure coupled with a piezoelectric actuator. Eur Phys J Plus 2019;134:1–23.#307.
[8] Martin CR. Membrane-based synthesis of nanomaterials. Chem Mater 1996;8:1739–46.
[9] Bakhtiari-Nejad F, Nazemizadeh M. Size-dependent dynamic modeling and vibration analysis of MEMS/NEMS-based nanomechanical beam based on the nonlocal elasticity theory. Acta Mech 2016;227:1363–79.
[10] Habibi M, Mohammadgholiha M, Safarpour H. Wave propagation characteristics of the electrically GNP-reinforced nanocomposite cylindrical shell. J Braz Soc MechSci Eng 2019;41:1–15.
[11] Chatzigeorgiou G, Meraghni F, Javili A. Generalized interfacial energy and size effects in composites. J Mech Phys Solids 2017;106:257–82.
[12] Shen J, Wang H, Zheng S. Size-dependent pull-in analysis of a composite laminated micro-beam actuated by electrostatic and piezoelectric forces: generalized differential quadrature method. Int J Mech Sci 2018;135:353–61.
[13] Xia X, Du Z, Zhang J, Li J, Weng GJ. A hierarchical scheme from nano to macro scale for the strength and ductility of graphene/metal nanocomposites. Int J Eng Sci 2021;162:1–20.# 103476.
[14] Lu L, She G-L, Guo X. Size-dependent postbuckling analysis of graphene reinforced composite microtubes with geometrical imperfection. Int J Mech Sci 2021;199:1–12.# 106428.
[15] Lee D, Nguyen DM, Rho J. Acoustic wave science realized by metamaterials. Nano Convergence 2017;4:1–15.# 3
[16] Zaera R, Vila J, Fernandez-Saez J, Ruzzene M. Propagation of solitons in a two-dimensional nonlinear square lattice. Int J Non Linear Mech 2018;106:188–204.
[17] Yang H, Timofeev D, Giorgio I, Müller WH. Effective strain gradient continuum model of metamaterials and size effects analysis. Continuum Mech Thermodyn 2020:1–23.
[18] Dunn M, Wheel M. Size effect anomalies in the behaviour of loaded 3dmechanical metamaterials. Philosophical Magazine (series 8) 2020;100:139–56.
[19] Mindlin RD. Microstructure in linear elasticity. Tech. Rep. Columbia Univ., New York, Dept. of Civil Engineering and Engineering Mechanics; 1963.
[20] Eringen AC. Linear theory of micropolar elasticity. J Math Mech 1966;15:909–23.
[21] Eringen AC, Edelen D. On nonlocal elasticity. Int J Eng Sci 1972;10:233–48.
[22] Toupin R. Elastic materials with couple-stresses. Arch Ration Mech Anal 1962;11:385–414.
[23] Fernández-Sáez J, Zaera R. Vibrations of Bernoulli-Euler beams using the two-phase nonlocal elasticity theory. Int J Eng Sci 2017;119:232–48.
[24] Romano G, Barretta R, Diaco M. On nonlocal integral models for elastic nano-beams. Int J Mech Sci 2017;131:490–9.
[25] Barretta R, Luciano R, de Sciarra FM, Ruta G. Stress-driven nonlocal integral model for Timoshenko elastic nano-beams. Eur J Mech-A/Solids 2018;72:275–86.
[26] Li L, Hu Y, Li X. Longitudinal vibration of size-dependent rods via nonlocal strain gradient theory. Int J Mech Sci 2016;115:135–44.
[27] Soltani D, Akbarzadeh Khorshidi M, Sedighi HM. Higher order and scale-dependent micro-inertia effect on the longitudinal dispersion based on the modified couple stress theory. J Comput Des Eng 2021;8(1):189–94.
[28] Hassanzadeh K, Farughi S. Longitudinal vibrations of functionally graded material nano-rod based on nonlocal strain gradient theory. J Mech Eng 2021;51:41–50.
[29] Jalaei M, Arani AG, Nguyen-Xuan H. Investigation of thermal and magnetic field effects on the dynamic instability of FG Timoshenko nanobeam employing nonlocal strain gradient theory. Int J Mech Sci 2019;161:1–11.# 105043.
[30] Zhang B, Li H, Kong L, Shen H, Zhang X. Coupling effects of surface energy, strain gradient, and inertia gradient on the vibration behavior of small-scale beams. Int J Mech Sci 2020;184:1–21.# 105834.
[31] Esen I. Dynamics of size-dependant Timoshenko micro beams subjected to moving loads. Int J Mech Sci 2020;175:1–11.# 105501.
[32] Abdelrahman AA, Esen I, Özarpa C, Eltaher MA. Dynamics of perforated nanobeams subject to moving mass using the nonlocal strain gradient theory. Appl Math Model 2021;96:215–35.
[33] Gholami R, Darvizeh A, Ansari R, Sadeghi F. Vibration and buckling of first-order shear deformable circular cylindrical micro-/nano-shells based on Mindlin's strain gradient elasticity theory. Eur J Mech-A/Solids 2016;58:76–88.
[34] Hosseini-Hashemi S, Sharifpour F, Ilkhani MR. On the free vibrations of size-dependent closed micro/nano-spherical shell based on the modified couple stress theory. Int J Mech Sci 2016;115:501–15.
[35] Ghorbani K, Rajabpour A, Ghadiri M. Determination of carbon nanotubes size-dependent parameters: molecular dynamics simulation and nonlocal strain gradient continuum shell model. Mech Based Des Struct Mach 2021;49:103–20.
[36] Mohammadimehr M, Navi BR, Arani AG. Modified strain gradient Reddy rectangular plate model for biaxial buckling and bending analysis of double-coupled piezoelectric polymeric nanocomposite reinforced by FG-SWNT. Compos Part B 2016;87:132–48.
[37] Nematollahi MS, Mohammadi H. Geometrically nonlinear vibration analysis of sandwich nanoplates based on higher-order nonlocal strain gradient theory. Int J Mech Sci 2019;156:31–45.
[38] Liu C, Yu J, Xu W, Zhang X, Wang X. Dispersion characteristics of guided waves in functionally graded anisotropic micro/nano-plates based on the modified couple stress theory. Thin-Walled Struct 2021;161:1–11.# 107527.
[39] Bacigalupo A, Gambarotta L. Identification of non-local continua for lattice-like materials. Int J Eng Sci 2021;159:1–21.# 103430.
[40] Polyzos D, Fotiadis D. Derivation of mindlins first and second strain gradient elastic theory via simple lattice and continuum models. Int J Solids Struct 2012;49:470–80.
[41] Gómez-Silva F, Fernández-Sáez J, Zaera R. Nonstandard continualization of 1D lattice with next-nearest interactions. low order ODEs and enhanced prediction of the dispersive behavior. Mech Adv Mater Struct 2020:1–10.
[42] Challamel N, Zhang Z, Wang C, Reddy J, Wang Q, Michelitsch T, et al. On nonconservativeness of Eringens nonlocal elasticity in beam mechanics: correction from a discrete-based approach. Arch Appl Mech 2014;84:1275–92.
[43] Challamel N, Zhang Z, Wang C. Nonlocal equivalent continua for buckling and vibration analyses of microstructured beams. J Nanomech Micromech 2015;5:A4014004.
[44] Challamel N, Picandet V, Elishakoff I, Wang CM, Collet B, Michelitsch T. On nonlocal computation of eigenfrequencies of beams using finite difference and finite element methods. Int J Struct Stab Dyn 2015;15:1–18.# 1540008.
[45] Wang CM, Zhang Z, Challamel N, Duan WH. Calibration of Eringen's small length scale coefficient for initially stressed vibrating nonlocal Euler beams based on microstructured beam model. J Phys D 2013;46:345501.
[46] Wang CM, Zhang H, Gao R, Duan W, Challamel N. Hencky bar-chain model for buckling and vibration of beams with elastic end restraints. Int J Struct Stab Dyn 2015;15:1–16.# 1540007.
[47] Bacigalupo A, Gambarotta L. A dynamic high-frequency consistent continualization of beam-lattice materials. Compos Struct 2021:1–8.# 114146.
[48] Gómez-Silva F, Zaera R. Analysis of low order non-standard continualization methods for enhanced prediction of the dispersive behaviour of a beam lattice. Int J Mech Sci 2021;196:1–11.#106296.
[49] Gómez-Silva F, Zaera R. Low order nonstandard continualization of a beam lattice with next-nearest interactions: enhanced prediction of the dynamic behavior. Mech Adv Mater Struct 2021:1–15.
[50] Duan WH, Challamel N, Wang CM, Ding Z. Development of analytical vibration solutions for microstructured beam model to calibrate length scale coefficient in nonlocal timoshenko beams. J Appl Phys 2013;114:1–11.# 104312.
[51] Zhang Z, Challamel N, Wang CM. Eringen's small length scale coefficient for buckling of nonlocal Timoshenko beam based on microstructured beam model. J Appl Phys 2013;114:1–6.# 114902.

[52] Barchiesi E, Dell'Isola F, Bersani AM, Turco E. Equilibria determination of elastic articulated duoskelion beams in 2D via a Riks-type algorithm. Int J Non Linear Mech 2021;128:1–24.# 103628.
[53] Vangelatos Z, Melissinaki V, Farsari M, Komvopoulos K, Grigoropoulos C. Intertwined microlattices greatly enhance the performance of mechanical metamaterials. Math Mech Solids 2019;24:2636–48.
[54] Jamshidian M, Boddeti N, Rosen D, Weeger O. Multiscale modelling of soft lattice metamaterials: micromechanical nonlinear buckling analysis, experimental verification, and macroscale constitutive behaviour. Int J Mech Sci 2020;188:1–20. # 105956.
[55] Bai L, Gong C, Chen X, Sun Y, Xin L, Pu H, Peng Y, Luo J. Mechanical properties and energy absorption capabilities of functionally graded lattice structures: experiments and simulations. Int J Mech Sci 2020;182:1–12.# 105735.
[56] Turco E, Barchiesi E, Giorgio I, Dell'Isola F. A Lagrangian Hencky-type non-linear model suitable for metamaterials design of shearable and extensible slender deformable bodies alternative to timoshenko theory. Int J Non Linear Mech 2020; 123:1–19.# 103481.
[57] Marino E, Hosseini SF, Hashemian A, Reali A. Effects of parameterization and knot placement techniques on primal and mixed isogeometric collocation formulations of spatial shear-deformable beams with varying curvature and torsion. Comput Math Appl 2020;80:2563–85.
[58] Turco E, Barchiesi E, dell'Isola F. A numerical investigation on impulse-induced nonlinear longitudinal waves in pantographic beams. Math Mech Solids 2021: 1–27.# 10812865211010877.
[59] Chaterjee S, Pohit G. A large deflection model for the pull-in analysis of electrostatically actuated microcantilever beams. J Sound Vib 2009;322:969–86.
[60] Dai H, Wang L. Size-dependent pull-in voltage and nonlinear dynamics of electrically actuated microcantilever-based mems: a full nonlinear analysis. Commun Nonlinear Sci Numer Simul 2017;46:116–25.
[61] Hanay MS, Kelber SI, O'Connell CD, Mulvaney P, Sader JE, Roukes ML. Inertial imaging with nanomechanical systems. Nat Nanotechnol 2015;10:339–44.
[62] Dilena M, Dell'Oste MF, Fernández-Sáez J, Morassi A, Zaera R. Hearing distributed mass in nanobeam resonators. Int J Solids Struct 2020;193:568–92.
[63] Andrianov I, Awrejcewicz J, Weichert D. Improved continuous models for discrete media. Math Probl Eng 2010;2010:1–35.# 986242.
[64] Bacigalupo A, Gambarotta L. Generalized micropolar continualization of 1D beam lattices. Int J Mech Sci 2019;155:554–70.
[65] Rosenau P. Hamiltonian dynamics of dense chains and lattices: or how to correct the continuum. Phys Lett A 2003;311:39–52.
[66] Rosenau P, Schochet S. Compact and almost compact breathers: a bridge between an anharmonic lattice and its continuum limit. Chaos 2005;15:1–18.# 015111.
[67] Santoro R, Elishakoff I. Accuracy of the finite difference method in stochastic setting. J Sound Vib 2006;291:275–84.
[68] Challamel N, Wang C, Elishakoff I. Discrete systems behave as nonlocal structural elements: bending, buckling and vibration analysis. Eur J Mech-A/Solids 2014;44: 125–35.
[69] Cazzani A, Stochino F, Turco E. On the whole spectrum of Timoshenko beams. part i: a theoretical revisitation. Zeitschrift für angewandte Mathematik und Physik 2016;67:1–30.# 24
[70] Cazzani A, Stochino F, Turco E. On the whole spectrum of Timoshenko beams. part ii: further applications. Zeitschrift für angewandte Mathematik und Physik 2016; 67:1–21.# 25
[71] Metrikine AV, Askes H. One-dimensional dynamically consistent gradient elasticity models derived from a discrete microstructure: Part 1: generic formulation. Eur J Mech-A/Solids 2002;21:555–72.
[72] Hussein MI, Leamy MJ, Ruzzene M. Dynamics of phononic materials and structures: historical origins, recent progress, and future outlook. Appl Mech Rev 2014;66:1–38.# 040802.
[73] Gómez-Silva F, Zaera R. Novel Enriched Kinetic Energy continuum model for the enhanced prediction of a 1D lattice with next-nearest interactions. Compos. Struct. 2021:1–13. https://doi.org/10.1016/j.compstruct.2021.115003.# 115003.